ELSEVIER

Contents lists available at ScienceDirect

## Chemical Engineering Science

journal homepage: www.elsevier.com/locate/ces



# A critical comparison of Pb-loaded organosilica and ion-exchange resins, with bispicolylamine ligands, for adsorption of iodide: Evidence of a 'matrix effect' on uptake properties

Thomas J. Robshaw <sup>a,b,\*</sup>, Fiona M. Lambert <sup>b,c</sup>, Sophie D. Watson <sup>b,d</sup>, Supakorn Tantisryanurak <sup>e,f</sup>, Nuha Mukhtar <sup>b</sup>, Victoria Shields <sup>b</sup>, Joshua Turner <sup>g</sup>, Robert Dawson <sup>e</sup>, Brant Walkley <sup>b</sup>, Clint A. Sharrad <sup>h</sup>, Mark D. Ogden <sup>b,i</sup>

- <sup>a</sup> School of Chemical & Process Engineering, University of Leeds, Woodhouse, Leeds, West Yorkshire, United Kingdom
- b School of Chemical, Materials & Biological Engineering, University of Sheffield, Sheffield, South Yorkshire, United Kingdom
- <sup>c</sup> Dept. Engineering & Maintenance, Sellafield Ltd., Seascale, Cumbria, United Kingdom
- d Westinghouse Electric Company UK Ltd., Springfields, Salwick, Preston, Lancashire, United Kingdom
- <sup>e</sup> School of Mathematical & Physical Sciences, University of Sheffield, Sheffield, South Yorkshire, United Kingdom
- f Mahidol Wittayanusorn School, Nakhon Pathom, Thailand
- <sup>8</sup> National Nuclear Laboratory, Central Laboratory, Seascale, Cumbria, United Kingdom
- <sup>h</sup> Dept. Chemical Engineering, University of Manchester, Manchester, United Kingdom
- <sup>i</sup> Nuclear Futures Institute, Bangor University, Dean Street, Bangor, Gwynedd, United Kingdom

#### ARTICLE INFO

#### Keywords: Adsorption Ion-exchange Iodine-129 Metal-loaded resin Organosilica Bispicolylamine

## ABSTRACT

Ion-exchange resins currently rely upon petrochemicals for their manufacture. Alternative materials are under consideration to create adsorbents for selective removal of ions from water. However, there has been little investigation of the impact on these adsorbent chemistries on the resulting fundamental adsorption behaviour. Presented here is an investigative comparison of metal-loaded polymeric and silica-based adsorbents for the remit of selective radioiodine (in the form of iodide) capture, using lead ions, chelated by bispicolylamine (BPA) ligands to create iodide affinity. The results indicate marked differences in uptake behaviour between the two materials. The ion-exchange resin (M4195-Pb) displayed more thermodynamically-favourable iodide capture, with a calculated uptake of 338  $\pm$  12 mg g $^{-1}$ , and retained some selectivity in the presence of acid, and 10 molar equivalents of nitrate and molybdate. The silica had much lower capacity of 46.5  $\pm$  7.6 mg g $^{-1}$ , but adsorbed extremely rapidly, reaching near capacity in <1 min. Generally, the binding of both Pb $^{2+}$  and iodide were significantly destabilised by the silica matrix, which was attributed primarily to a H-bonding interaction between the BPA ligand and the adsorbent surface. It did however, result in generally better thermal stability of the bound iodide. This appears to be the first report of this nature into this 'matrix effect' phenomenon and demonstrates that great care is required in the future design of ion-exchange and adsorption media using alternate support chemistries.

## 1. Introduction

Polymeric ion-exchange (IX) resins are generally regarded as the 'go to' technology for a selective chemical separation process, where the target species is present in an aqueous stream, at mg  $\rm L^{-1}$  concentrations. Resins offer economical manufacture, chemical and physical robustness, consistent particle size/characteristics and amenability with standard hydrodynamic column setups (Alexandratos, 2009). They are commonly

produced using a styrene/divinylbenzene or acrylic/divinylbenzene matrix and bestowed with a large array of functional groups, including chelating ligands. These can be highly-selective for certain ions, dependant on factors such as cavity size and hard-soft-acid-base behaviour (Chiarizia et al., 1998; Wilson et al., 2013; Robshaw et al., 2019). Selectivity towards anions with organic ligands is generally harder to achieve and is in less demand industrially; since the great majority of valorisable aqueous ions are metal cations (Bezzina et al.,

E-mail address: t.j.robshaw@leeds.ac.uk (T.J. Robshaw).

https://doi.org/10.1016/j.ces.2025.122799

<sup>\*</sup> Corresponding author.

2018; Shields et al., 2023). Anion selectivity can be achieved by first loading a cation onto the chosen adsorbent, which then enjoys high affinity with certain anions, which are uptaken by ligand-exchange, rather than IX. This strategy has been known and employed with respect to fluoride ions for several decades (He et al., 2020; Ni et al., 2022).

A fundamental problem facing IX resins for the future is that they are manufactured from petrochemical-based, non-renewable resources. While it is accepted that most environmental impact and carbon footprint of IX systems come from the chemicals used to elute and regenerate the columns (Choe et al., 2013), the production of bulk styrene produces a considerable quantity of  $CO_2$  ( $\leq 7.38$  kg  $CO_2$  kg $^{-1}$  product (Amini et al., 2015). IX resins also have no concerted recycling process at the end of their operational life and are frequently either simply landfilled or combusted (Atkinson et al., 2025). For this reason, there has been much recent research into more inherently sustainable adsorbent chemistries, including extractants synthesised from renewable feed-stocks (Song et al., 2017; Zia et al., 2020) and those derived from waste materials produced from other industries, including polystyrene itself (Tran et al., 2020).

There are other reasons to consider alternative adsorbent matrices. For example, in the case of the nuclear industry. Here, effective waste management is crucial to ensure the continuing prosperity of the industry, not least in terms of social acceptability. The release of radionuclides into the environment is under considerable scrutiny. The Nuclear Energy Agency (NEA) have urged that all new nuclear design and technology should aim for "near zero" radionuclide emissions by 2050 (NEA, 2018).

In terms of overall dose contribution, upon environmental release, iodine-129 is a radionuclide of high concern (Turner, 2021). A variety of iodine-bearing aqueous wastestreams are created by nuclear fuel recycling operations, both by dissolution of the spent fuel in 9 M HNO3 and the capture of off-gas condensate by both acidic and caustic scrubbing, with the iodine being present mainly in anionic form (Robshaw et al., 2021). There is currently no deployed industrial process to capture and contain the I-129 from these streams. However, one solution is direct adsorption and concentration within a solid phase, which can then be encapsulated, in a relatively low-volume wasteform, and stored geologically. Accordingly, any potential adsorbent needs to be assessed holistically; not just in terms of its ability to uptake iodine in industrially relevant conditions, but also its compatibility with the final wasteform (Asmussen et al., 2022). The adsorbent matrix, as well as the chemical functionality that interacts with the iodine, is thus of importance. To this point, IX resins offer limited compatibility with cementation (Atkinson et al., 2025; Wang and Wan, 2015). Silica-based extractants have attracted interest for this remit in recent years, due to the perceived compatibility of SiO2 with Portland cement mix (Kearney et al., 2022; Simoni et al., 2024).

Regardless of one's motive for considering an alternate adsorbent material, it is important that the effect of the material's chemical properties on the adsorption parameters themselves is understood and quantified. This allows any required modifications to be made to the engineering setup, when converting from an IX resin to an alternative, in advance, improving plant efficiency. These could include adsorbent bed volume, flow-rate and choice of eluent.

There is a plethora of research exploring ligand and functional group choice, with a view to gaining the required selectivity for a chemical species (Alexandratos, 2009; Robshaw et al., 2022; Silva et al., 2021). However, there has been, to our knowledge, not one concerted review published, exploring the implications of adsorbent matrix chemistry. This is despite several examples in the literature of significant differences in uptake behaviour between two adsorbents possessing the same functional group. For example, a hypercrosslinked polymer, functionalised with sulfonic acid groups, was shown to be more selective for Cs and Sr than a similarly functionalised metal organic framework (MOF) (Aguila et al., 2016; James et al., 2019). In a comparison between an

organosilica and IX resin, both containing phosphonic acid-based ligands, it was found that the silica exhibited less thermodynamically-favourable adsorption of  $\mathrm{Sr}^{2+}$ , yet much faster kinetics (Pepper et al., 2018). In a comparison of two biphenol-based microporous polymers, it was found that even seemingly small differences in the placement of phenol groups, relative to the repeating polymer unit, produced large differences in pore characteristics and ensuing mechanisms of uptake of fluoride (Robshaw et al., 2020). In these mentioned studies, a number of factors were postulated to be responsible for these interesting differences in performance. These included hydrophobicity of the matrix, pore size and placement of the functional groups (particle surface verses pore-interior). However, these predictions were mainly speculative, rather than based on empirical data.

The purpose of the current study therefore, is to make a systematic and critical comparison between two adsorbents of equivalent functionality, but very different matrix chemistry. The context of the comparison will be the removal of iodide from aqueous solutions, with a view to produce an active, loaded adsorbent, subsequently to be converted to a wasteform. The novelty of the work is to investigate and attempt to rationalise the differences in iodide-uptake behaviour to a level of detail that has previously not been illustrated.

The chemical conditions in which such adsorbents must operate are often very hostile, with high ionic strength, extreme pHs and high concentrations of competing anions (Decamp and Happel, 2013; Asmussen et al., 2019). IX resins have been researched extensively for use as radioiodine capturers; being employed sometimes in unmodified form, with amine or ammonium functionality. These materials offer high adsorption capacity of >500 mg g<sup>-1</sup>, but are often vulnerable to competition from macro concentrations of other ions and/or poor selectivity for iodate (Asmussen et al., 2022; Barton et al., 2019). Organosilicas with anion-exchange groups are also known for their iodine removal properties. A polyethyleneimine-impregnated silica is known to uptake >2 g g<sup>-1</sup> of gaseous and organic iodine (Hijazi et al., 2019). A pyridinium-functionalised silica was shown to have better aqueous iodide retention than strong base IX resins in column operation (Ye et al., 2019). However, experiments were not run in conditions relevant to nuclear effluents. It must also be born in mind that the point with most unmodified IX media is for the adsorption process to be reversible, allowing for regeneration; whereas for radioiodine, a 'oncethough' system, with geological disposal of the material is the more common strategy. Therefore near irreversible adsorption is preferable (Simoni et al., 2024; Asmussen et al., 2019).

Generally, for this remit, a highly selective functionality is called for and a similar approach to that applied to fluoride can be taken, by immobilising 'soft' metal ions onto a solid support. In previous work, a popular choice of loading metal for researchers has been Ag (AgI K<sub>sp</sub> =  $8.52 \times 10^{-17}$ ) (Robshaw et al., 2021). In a recent comparison of iodide removal performance, in challenging, acidic conditions, an Ag-loaded IX resin produced a distribution coefficient of  $>10^9$ , which was >4 orders of magnitude higher than for Cu, Bi or Pb (Robshaw et al., 2022). A large body of work has been amassed by researchers at Pacific Northwest National Laboratories (PNNL) on development of Ag-loaded silica 'hydrogels' (Asmussen et al., 2019; Matyas et al., 2011). These have demonstrated iodine removal from off-gas condensate wastewater and importantly, are compatible with geological disposal (Asmussen et al., 2019). Nonetheless, Ag is an increasingly expensive and important precious metal and it is debatable whether burying large masses of it in geological repositories constitutes efficient resource use. Ag is also labile with respect to oxidation state, meaning that adsorbents may have to be treated with UV light, or used in a closed system to avoid significant chemical changes (Liu et al., 2015; Mao et al., 2016) Other loading metals that have performed well in comparative studies include Bi and Ce, which were shown to remove iodide and iodate concurrently from a carbonate-rich alkaline solution, whereas Ag-loaded materials did not extract significant iodate (Asmussen et al., 2023). The multivalence of these metal ions compared to Ag is potentially attractive, as adsorbents

can theoretically immobilise more iodide/iodate anions per metal centre, thereby increasing efficiency. There is similarly potential worth in investigation of Hg adsorbents for radioiodine capture, as  $\mathrm{HgI}_2$  is also highly stable. Although the extreme toxicity of Hg is problematic.

Another multivalent metal less commonly investigated for this purpose is Pb (PbI<sub>2</sub>  $K_{sp} = 4.41 \times 10^{-9}$ ), with the only significant material reported in the literature being a hybrid Bi/Pb mineral adsorbent (Kodama, 1999). The major issue with this material was its lack of porosity, meaning only surface metal sites were gainfully utilised for iodide capture (again, this demonstrates the importance of consideration of the physicochemical properties of the adsorbent particles) (Kodama, 1999). Nonetheless, in the previously-mentioned comparison study, a Pb-loaded resin was the 4th best-performing adsorbent overall in terms of iodide capacity in challenging chemical conditions (Robshaw et al., 2022). Pb salts containing iodine species are known to have some resistance to leaching, when incorporated in cement or bitumen wasteforms; though less so than the more insoluble salts formed by Ag (Kalinin et al., 1983). Pb of course has high human and environmental toxicity compared to its competitors. However, this is arguably a less significant barrier for the nuclear industry, as the main hazard would be the radioactivity of the adsorbent/wasteform and control measures would already be elevated because of this. Pb is also economical and abundant compared to Ag.

The bispicolylamine (BPA) functionality is an attractive target for metal functionalisation and use with active wastestreams. It possesses delocalised pi electrons and contains no larger atoms prone to radiolytic attack, unlike other chelating functionalities (thiourea, aminophosphonic acid). This infers better long-term stability of the final wasteform (Ferry and Ngono, 2021). In previous work, a BPA IX resin, functionalised with Cu<sup>2+</sup> ions demonstrated promising iodide removal performance (CuI  $\rm K_{sp}=1.10\times10^{-12}$ ), However, this system was hampered by an in-situ REDOX reaction occurring between Cu<sup>2+</sup> and iodide, which oxidised the iodide to more volatile and weakly-bound species (Robshaw et al., 2020). We have therefore selected Pb as our loading metal of choice, which has a more stable 2+ oxidation state.

In terms of comparative adsorbent chemistries, we have selected a typical styrene/divinylbenzene IX resin, as it is a commercially available material, with the BPA functionality installed, in the form of DOWEX® M4195 (Table S1). The analogous organosilica can be synthesised in a facile  $S_N2$  reaction, with a ligand of one's choice, from commercially-available halopropyl silicas (Scheme 1). Metalation can then proceed by simply immersing the adsorbent in an aqueous solution of metal ions, which then coordinate bond to the BPA group (Scheme 1).

This creates a novel material, for which physicochemical properties and uptake parameters are unknown. Silica, as previously mentioned, also offers potential greater compatibility with final wasteform options. It is hoped the resulting comparison will build towards a 'toolkit' for understanding the impact of adsorbent chemistry on ion uptake characteristics and progress the design of the next generation of adsorption media.

#### 2. Methods

# 2.1. Synthesis of bispicolylpropylamine-functionalised silica gel (BPPrAsil)

All reagents were of analytical grade or better. A two-necked, round-bottom flask, fitted with a magnetic stirrer, was charged with 200–400 mesh 4-bromopropyl-functionalised silica gel (Table S2), hereafter referred to as 4-BrPrsil (8.643 g, 12.96 mmol functional group equivalent, calculated from manufacturer quote of 1.5 mmol g $^{-1}$ ) and anhydrous Na $_2$ CO $_3$  (5 g). This was placed under nitrogen and evacuated 3 times. Acetonitrile (99.9 %, 250 mL) was added anhydrously, followed by bispicolylamine (97 %, 2.40 mL, 13.33 mmol). The mixture was heated to 100 °C and refluxed, with stirring, for 18 hr. The product was washed with further acetonitrile, ethanol and deionised water until the filtrate pH was neutral. It was finally dried in a vacuum oven at 50 °C for 24 h, which afforded BPPrAsil as a light orange powder (yield: 8.401 g).

#### 2.2. Conditioning of adsorbents

A mass of 5 g BPPrAsil or DOWEX M4195 resin (as received from the manufacturer in partially hydrated form) was contacted with HNO $_3$  (1 M, 250 mL) and equilibrated in an orbital shaker for 24 hr. The resin/silica was then rinsed slowly with deionised water (500 mL). M4195 resin and derivatives were handled in hydrated form in all loading and uptake experiments. The dry mass equivalent was determined by calculating the loss of mass upon drying (SI, p2). The silica was dried in a vacuum oven at 50  $^{\circ}$ C for 24 h and handled in anhydrous form.

# 2.3. Determination of pseudo-acid dissociation constants for BPPrAsil and DOWEX M4195 resin

A sub-sample of M4195 was dried in an airflow oven at 80 °C for 24 hr and ground to a power in a pestle and mortar. MilliQ water, of resistivity  ${>}18~M\Omega$  was used throughout these experiments, to negate the influence of carbonic acid/carbonate. Samples of the resin (0.100 g), or functionalised silica (0.600 g), were suspended in standardised HNO3 (0.107 M, with sufficient NaNO3 to achieve ionic strength of 1.0 M). The suspensions were titrated, in a closed system, with a constant temperature of 21 °C, against NaOH (1.021 M), using a Mettler Toledo DL15 Potentiometric Titrator. Titrations were performed in triplicate, in static mode, with NaOH additions of 0.10 mL, with no experiment lasting longer than 20 min to reach the equivalence point. The resulting

**Scheme 1.** Showing the syntheses of the adsorbents featured in this work. "ACN" = acetonitrile.

potentiometric curves were fit using Microsoft Excel, using Billo's method for polyprotic analytes (Billo, 2004). Models accounting for 1–5 pK<sub>a</sub>s were used for data-fitting. The allowed variables were pK<sub>a</sub> values and ligand concentration. [HNO<sub>3</sub>] and [NaOH] were allowed to be adjusted to  $\pm 5$ % of the value calculated by standardisation. Error values were calculated using the Excel SolvStat add-in, again as per Billo's method (Billo, 2004).

#### 2.4. Functionalisation of BPPrAsil and DOWEX M4195 resin with Pb ions

To load the adsorbents with  $Pb^{2+}$  ions, 6.0 g (dry mass equivalent) of BPPrAsil or M4195 was contacted with  $Pb(NO_3)_2$  solution (250 mL, 0.1 M) and equilibrated in an orbital shaker for 24 hr. The metalated adsorbent was separated from the residual solution by gravity filtration and washed slowly with 500 mL deionised water. In the case of the silica, the material was dried in an airflow oven at 80 °C for 24 hr. This afforded the Pb-loaded forms of the adsorbents, which will be designated as BPPrAsil-Pb and M4195-Pb. The Pb concentration within each adsorbent was calculated by acid digestion of dried subsamples ( $\sim$ 0.5 g) in HNO<sub>3</sub>/HClO<sub>4</sub>.

#### 2.5. Iodide capture investigations from various media

All reagents were of analytical grade or better. All experiments were conducted in duplicate and uncertainty values were calculated from 2 x the standard deviation. In a typical experiment, the adsorbent ( $\sim$ 50 mg dry mass equivalent) was weighed into a glass vial and contacted with a precise volume of NaI solution. The vial was carefully equilibrated in an orbital shaker for 24 hr. Iodide uptake by the adsorbent was calculated by measurement of the iodide concentration in the pre-contact and post-contact solution by potentiometry or ion chromatography, then mass-balancing (SI, p3). In some experiments, controlled quantities of NO<sub>3</sub> and MoO<sub>4</sub><sup>2</sup> ions were added. In experiments to determine theoretical maximum iodide uptake, the data were fitted with a number of common two-parameter isotherm models (SI, p4).

For pH-controlled experiments, the suspensions were first made up to close to their intended final volume (25 mL) with deionised water, followed by addition of a defined volume of concentrated NaI from a stock solution (such that the iodide concentration of the solution, at final volume, would equal  $100 \text{ mg L}^{-1}$ ). The solution pHs were then adjusted with the minimum required quantities of HNO<sub>3</sub> and/or NaOH. The vials were equilibrated in an orbital shaker for at least 24 hr, with periodical pH adjustments, as previously described, to maintain the intended solution pH until equilibrium was reached. The samples were made up to their intended final volume, whilst maintaining the required pH, and an aliquot was separated from the adsorbent for analysis. For samples at the extreme ends of the pH scale, where pH could not be measured accurately by potentiometry, contact solutions were prepared using standardised HNO3 or NaOH solutions, also containing the required concentration of NaI. Aliquots of contact solutions were standardised again after adsorption equilibrium and it was confirmed that any pH change was negligible. The relevant proton concentrations for equilibrated samples were: pH 0 = 1.005 M, pH 1 = 0.0998 M. The relevant hydroxide concentrations were: pH 13 = 0.1003 M, pH 14 = 0.996 M.

For kinetic experiments, a mass of  $\sim$ 200 mg adsorbent was weighed into a large glass container, fitted with a magnetic stirrer bar and closable lid. This was contacted with a starting volume of 1.00 L NaI solution (1000 mg L $^{-1}$ ) and a timer was immediately started. Periodically, 2.000 mL volumes were removed from the container, using a pipette equipped with filtered tips and these were conserved for analysis. The maximum volume removed from the container was <25 mL. Data were fitted to commonly used kinetics models (SI, p5) and also tested for nonnormality and non-randomness, as per Revellame *et al.* (Revellame *et al.*, 2020).

#### 2.6. Solid-state analysis of the materials at various process stages

Samples were prepared for analysis first by washing with deionised water (>100 mL) to remove any residual contact solution. They were then dried in an airflow oven at 80  $^{\circ}\text{C}$  for 24 hr and, in the case of M4195 and derivatives, ground to a fine powder with a pestle and mortar. Some samples for solid-state analysis were treated with a mixed NaI/I2 solution, made by dissolving the relevant species in deionised water at a molar ratio of 1:6. Although one of the objectives in this work was to minimise the formation of triiodide in the uptake process, it was of interest to study the response of the materials in a diiodine/triiodidedominated system.

Elemental analysis (C, H, N and S) was performed using an Elementar Vario MICRO Cube CHN/S analyser. Fourier-transform infra-red (FTIR) spectroscopy was performed using a Spectratech IRAffinity-1S, with a Specac ATR attachment. Measurements were taken in transmission mode

Gas sorption parameters were attained using a Micromeritics ASAP 2020Plus analyser. Nitrogen sorption measurements were analysed at -196 °C using ~100 mg of sample. BET surface areas were calculated over a relative pressure range of 0.01–0.11P/P<sub>0</sub>. All samples were analysed in duplicate and average values and 2× standard deviations were calculated for each material, with errors propagated accordingly. Differential pore sizes were calculated using the NLDFT method using the model for carbon slit (M4195) or bucket-shaped (silicas) pores. Samples were degassed at 120 °C (M4195) and 80 °C (silicas) under dynamic vacuum immediately prior to analysis (it was found that higher temperatures caused degradation of the functional groups). Thermogravimetric analysis (TGA) was attained using a Perkin Elmer Pyris1. Samples (~6 mg) were weighed into a ceramic crucible and heated from ambient to 100  $^{\circ}\text{C}$  at a rate of 50  $^{\circ}\text{C}$  min  $^{-1}$  , held at 100  $^{\circ}\text{C}$  for 10 min, then heated from 100  $^{\circ}\text{C}$  to 800  $^{\circ}\text{C}$  at 50  $^{\circ}\text{C}$  min  $^{-1}.$   $N_2$  was used as the carrier gas. Xray diffraction (XRD) analysis was carried out using a Bruker D2 Phaser X-ray diffractometer, employing dual Ni K-β filters. Diffractograms were matched using the International Centre for Diffraction Data (ICDD) PDF-4 + database (Song et al., 2012).

X-ray photoelectron spectroscopy (XPS) was carried out using a Kratos Supra spectrometer, with a monochromated Al source and two analysis points per sample (full operating parameters in SI, p6).

#### 3. Results and discussion

# 3.1. Synthesis, functionalisation and elemental characterisation of materials

The microanalysis indicated  $\sim$  37 % successful functionalisation of BrPrsil, which was surprisingly low, since the functionalising BPA molecules should theoretically have been easily able to access the mesopores. For M4195, it was not possible to calculate an accurate BPA group concentration, because of the partial protonation of the functional group (meaning the contribution of nitrate to the N mass% could not be quantified) and presence of residual sulphate counteranions (Robshaw et al., 2020) (Table 1). Nonetheless, it is clear for both media that Pb ions are not loaded with a 1:1 stoichiometry with the functional group and are likely to be anchored in a variety of different microenvironments, with coordination to multiple BPA groups simultaneously, rather than chelating within a single BPA cavity. Indeed, it is known that Pb adsorption by M4195 resin is strongly pH-dependent, suggesting an ionexchange, rather than chelation mechanism is dominant (Diniz et al., 2002). To the best of our knowledge, there is no experimental or theoretical study exploring the precise mode of complexation between Pb<sup>2+</sup> ions and the BPA ligand and such work would be beneficial for future study of this system. Based on literature data (Robshaw et al., 2020), it is likely that M4195 loads more Pb<sup>2+</sup> ions per BPA functional group.

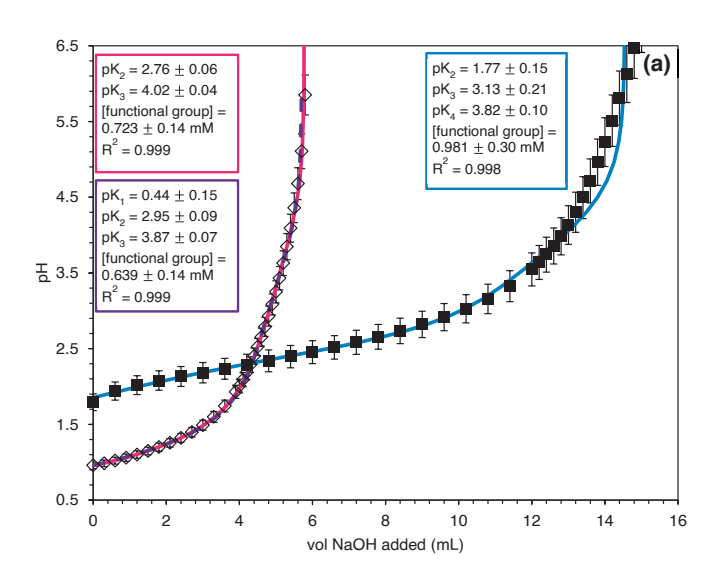
**Table 1**Elemental microanalysis data and derived functional group concentrations for resins and silica-based materials.

Material	Elemental composition (mass % and mmol g <sup>-1</sup> )										Calculated functional
	С		Н		N		S		Pb		group conc. (mmol $g^{-1}$ )
M4195 (HNO <sub>3</sub> conditioned)	65.9 ± 0.1	54.9 ± 0.1	6.14 ± 0.03	61.4 ± 0.3	11.0 ± 0.0	7.88 ± 0.01	$0.40\pm0.08$	$0.125 \pm 0.026$	-	-	$\#1.98 \pm 0.05$
M4195-Pb	$63.8 \pm \\0.1$	$53.2 \pm \\0.1$	$5.88 \\ \pm 0.01$	$58.8 \\ \pm 0.1$	$\begin{array}{c} 10.4\ \pm \\ 0.0 \end{array}$	$\begin{array}{c} 7.39 \pm \\ 0.00 \end{array}$	< 0.01	< 0.03	$^*12.6 \pm 0.1$	$^*0.606 \pm 0.003$	$*0.606 \pm 0.003$
4-BrPrsil	$*5.33 \pm 0.06$	*4.44 ± 0.05	$1.47 \\ \pm 0.03$	$14.7 \\ \pm 0.3$	< 0.01	< 0.07	< 0.01	< 0.03	-	_	$1.48\pm0.02$
BPPrAsil	$\begin{array}{c} 10.1 \; \pm \\ 0.0 \end{array}$	$\begin{array}{c} 8.39 \pm \\ 0.04 \end{array}$	$\begin{array}{c} 1.72 \\ \pm \ 0.01 \end{array}$	$17.2 \\ \pm 0.1$	$^*2.32 \pm 0.01$	$^*1.65 \\ \pm 0.01$	< 0.01	< 0.03	_	_	$0.551\pm 0.003$
BPPrAsil-Pb	$\begin{array}{c} \textbf{8.94} \pm \\ \textbf{0.04} \end{array}$	$\begin{array}{c} \textbf{7.45} \pm \\ \textbf{0.04} \end{array}$	$\begin{array}{c} 1.86 \\ \pm \ 0.04 \end{array}$	$18.6 \\ \pm 0.4$	$\begin{array}{c} \textbf{1.77}  \pm \\ \textbf{0.00} \end{array}$	$\begin{array}{c} 1.26\ \pm \\ 0.00 \end{array}$	< 0.01	< 0.03	$^{*2.53}_{\pm~0.08}$	$^{*0.122} \pm \\ 0.004$	$*0.122 \pm 0.004$

<sup>\*</sup> Indicates which element was used to calculate functional group concentrations.

# 3.2. Determination of pseudo-acid dissociation constants for M4195 and RPPrAsil

Fitting of titration data was attempted, using models for  $1-4~pK_{as}$ . For each adsorbent, the closest fitting model, which returned sensible values in the context of the functional group chemistry and known literature were chosen, and are presented in Fig. 1. For full dataset, see



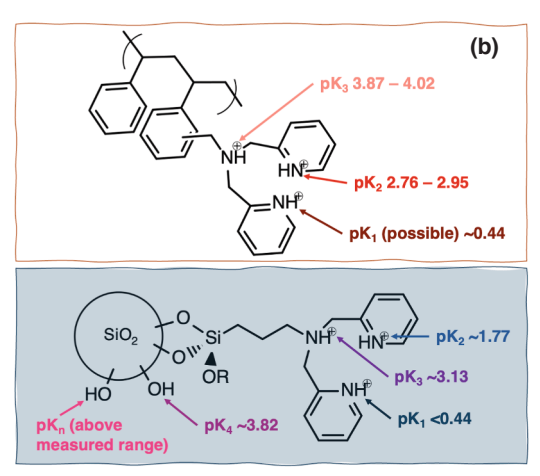


Fig. 1. (a) Potentiometric titration of suspensions of M4195 ( $\diamondsuit$ ) and BPPrAsil ( $\blacksquare$ ) in HNO<sub>3</sub> against NaOH and fitting of titration data using Billo's method for polyprotic systems (coloured lines). (b) Diagram showing the assigned pseudopK<sub>a</sub>s of the two materials.

SI, Table S3). For M4195, both di-protic and tri-protic models returned feasible values and fitting was almost identical. The tri-protic model takes into account a value for the most acidic BPA pK<sub>a</sub> (one of the aromatic amines), which may have been just outside the pH range of the experiment (known to be in the region of 0.5 in chloride media (Wolowicz and Hubicki, 2012). In any case, the other two predicted values were close to those predicted by the di-protic model. These are in turn fairly close to previously reported values of 2.1 and 4.13 for M4195 in chloride media (Ogden et al., 2017). It is known that the acidity of the BPA system specifically is quite sensitive to the counteranions present in solution (Diniz et al., 2002; Wolowicz and Hubicki, 2012). For BPPrAsil, the best-fitting sensible model was tri-protic. The most logical explanation is that the most basic pKa at 3.82 accounts for a proportion of the silanol groups on the adsorbent surface. Attempts to quantify the pK<sub>2</sub>s of silanol groups on silica particles are quite variable. However, the range for the most acidic type of silanol has been reported as  $\sim 3.8-5.5$ , representing ~ 15-20 % of the total fraction of silanol groups (Onizhuk et al., 2018). The fit of the model to the BPPrAsil data is poorest at pH 4.5-5, which suggests it cannot fully describe the contribution of silanol groups to the overall acidity. The limitation of the model used is that it assumes that the concentrations of all protic groups in the adsorbent material are equivalent (Billo, 2004), which may obviously not be the case here. Nonethless, there has been evidence to implicate an acidic silanol group in very similar experiments with ethyl/butylphosphonate silica (Pepper et al., 2018). If we allow the presence of the silanol group for these data, it follows that the other two model pKa values, of 1.77 and 3.13 are the equivalents of the measurable amine pKas in the M4195 experiment (Fig. 1(b)), being similar, but more acidic. The most acidic amine pKa is almost certainly not measurable for BPPrAsil as, by this logic, it would be rather lower than 0.5 (Wolowicz and Hubicki, 2012). Accounting for silanol group interaction would also explain why the calculated total functional group concentration is rather higher for the silica (Fig. 1(a)), even though it is seen from Table 1 that this is actually not the case, with respect to the BPA ligand.

Overall, protons appear to dissociate from the BPA groups at a lower pH in a silica matrix than for a polymeric resin. This is most likely because the unprotonated amines are stabilised through H-bond donation by adjacent silanol groups, which has been reported for multiple organosilanols (Lickliss and Sykes, 1995). It is well known that H-bonding interactions lower the pKa of a functional group (Thurlkill et al., 2006). Furthermore, Asenath-Smith & Chen reported a specific H-bonding interaction taking place between surface silanol groups and an aminopropylsilane ligand (Asenath-Smith and Chen, 2008). This illustrates some of the factors that require consideration when attaching a ligand to a hydrophilic, rather than hydrophobic adsorbent matrix. The effects on the stability of the ternary metal complexes formed upon Pb coordination were later found to be significant (Section 3.3.1).

FTIR spectra of the two adsorbents, at various relevant processing stages, are shown in Figs. S1 and S2, while all notable peaks are

<sup>#</sup>Approximate value for comparison, taken from reference (Robshaw et al., 2020). Not measured experimentally.

characterised in Table S4. For the resin samples, changes are seen between the protonated and Pb-loaded forms, concurrent with the coordination of the Pb ions, including the aromatic C–H stretch at  $\sim\!3000~{\rm cm}^{-1}$  and the aromatic C–C stretch region (1400–1500  ${\rm cm}^{-1}$ ). Notably, there was no change, for the resin spectra, in the N-H stretch region at  $\sim\!1750~{\rm cm}^{-1}$ , which is unlike the analogous Cu-loaded material (Robshaw et al., 2020). This may imply a low proportion of metalated iodide binding sites, due to incomplete Pb functionalisation (meaning that the amines can remain as protonated ammonium, as there is no lone pair donation to the metal centre). It likely also indicates that the large Pb ions coordinate differently to ions which can fit within the functional group 'cavity', without interaction with the aliphatic nitrogens (Diniz et al., 2002).

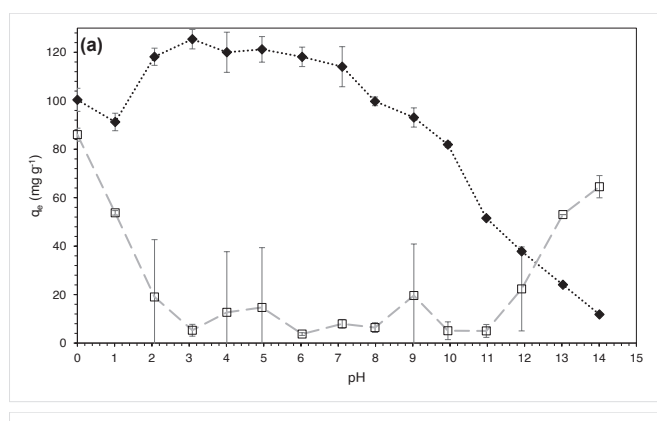
BPPrAsil spectra are largely featureless (Fig. S2), only showing the main peaks that would be expected from a silica-based sample and not revealing information about the organic fraction of the material. This has been previously observed for similar samples and we do not draw any conclusion on the success or failure of the functionalisation reaction based on FTIR data (Robshaw et al., 2023). The functionalisation is confirmed by elemental and XPS analysis (Table 1; Fig. 5(a)). There is however, an interesting weak peak at  $\sim 760~{\rm cm}^{-1}$ , which appears only upon iodide/iodine contact. This is in close proximity to the Si–O–Si vibration at  $\sim\!800~{\rm cm}^{-1}$  and is thought to indicate some deformation of the silica lattice, due to large triiodide anions associating with the organic ligand.

#### 3.3. Iodide uptake investigations, using various aqueous conditions

The focus of this work was on the performance of the metalated adsorbents. It should be noted that for proof of concept, we ran exploratory iodide uptake experiments, with non-metallated versions of the two materials and with the 4-BrPrsil starting material, with an initial [I<sup>-</sup>] of 2000 mg L<sup>-1</sup>. (Table S5) The non-metallated BPA-bearing materials exhibited similar, but lower iodide capacity to the metalated equivalents, while 4-BrPrsil produced an undetectable level of iodide adsorption. The non-metallated materials superficially show reasonable affinity for iodide anions, due to protonated ammonium groups in the BPA ligand acting as anion-exchange sites (Robshaw et al., 2020). In applied conditions, this would be completely negated by the macro concentrations of other anions (mainly nitrate) present in the system (Robshaw et al., 2023). For this reason, metal-loaded adsorbents dominate the literature on development of adsorption media for radioiodine. For a comparison to iodide removal from water by nonmetallated anion-exchange resins, the reader is directed to reference (Barton et al., 2019).

#### 3.3.1. pH-controlled experiments

The pH adsorption/leaching profiles (Fig. 2) illustrate how M4195 is the significantly more chemically-stable adsorbent under changing pH, as it maintains high capacity and relatively low Pb leaching over a pH range of 3-10. In contrast, the silica leaches an unexpectedly large amount of Pb at pH 6 and below; indicating that either the mode of Pb coordination is different (and weaker), or that the silica matrix is in some way detrimental to the stability of Pb binding. The data show the importance of an iodide-selective functionality, since, over the pH range 2–5, uptake by M4195-Pb remains high, as there is minimal Pb leaching. However, for the silica, the majority of Pb is leached and uptake of iodide decreases with pH, as the competition by nitrate for the nonselective protonated ammonium groups becomes more severe. It is noted that in neither case would the leached  $Pb^{2+}$  form  $PbI_{2(s)}$ , as  $PbI_2$  in soluble in NaI and KI solutions. Pb leaching in deionised water (without iodide) did not produce significant Pb leaching for either material (samples were below the limit of quantification). The water treatment works discharge limit for environmental permits is an average of 2 µg L<sup>-1</sup> in the United Kingdom. Table S6 illustrates how the resulting effluent from a batch separation process (for both adsorbents) would



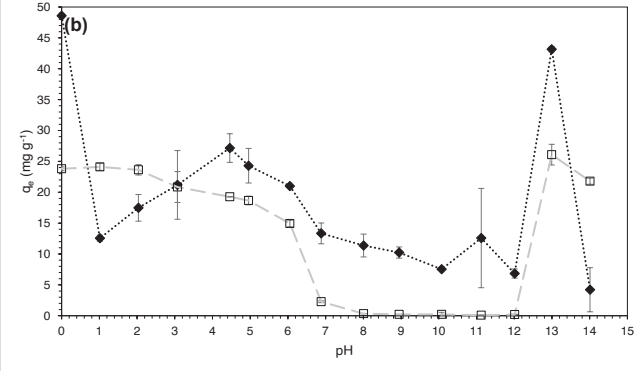


Fig. 2. Comparison of iodine uptake ( $\spadesuit$ ) and Pb leaching ( $\square$ ) for (a) M4195-Pb and (b) BPPrAsil-Pb over a pH range of 0–14. Adsorbent mass = 50 mg. Solution volume = 25 mL. Iodide concentration = 100 mg L $^{-1}$ . T = 20 °C. Y axis applies to both the mass of iodine taken up by the adsorbent and the mass of Pb leached from it. Note the difference in Y axis scale for the two adsorbents.

have a Pb concentration greatly in excess of this (range = 0.45–342 mg  $L^{-1}$ ), which is a clear issue for the potential deployment of Pb-loaded adsorbents for this remit.

The silica data do show a remarkable increase in iodide affinity at pH 0 and pH 13. At pH 0, the most acidic amine in the BPA functionality becomes protonated (Ogden et al., 2017), but this is unlikely to account for the large increase in iodide adsorption, compared to pH 1, because of competition from nitrate. Also, the increase does not tally with the proportion of extra binding sites that would be created. It is possible that the multiple silanol groups on the silica surface become protonated and positively-charged in the very acidic conditions and these would exist in sufficient concentration that significant iodide uptake might be achieved, even with the nitrate competition. This species has been identified in the literature at pH < 2 (Duval et al., 2002).

At pH 13 and 14, the solid silica matrix was completely hydrolysed and the silica would most likely exist in colloidal form in the sample solutions. It is theorised that at pH13, a solubilised BPA/Pb complex exists, which binds iodide strongly, while at pH 14, the iodide binding is overwhelmed by the hydroxide concentration. We investigated this via mass spectrometry and UV–Vis spectroscopy (experimental detail in SI, p7&10).

Mass spectrometry results were unfortunately inconclusive, as no peaks could be sensibly assigned to postulated chemical species. It is probable that the major detected species are of high molecular weight and multi-charged. The mass spectra of alkoxysilanes (which would be the most feasible hydrolysis product in this case) are widely recognised as being difficult to interpret, as such species commonly fragment in the mass spectrometer, displaying no molecular ion but rather base peaks indicative of fragmentation. Adamovich *et al.* studied functionalised, N-containing alkoxysilanes similar to the type of proposed breakdown products in this work (Adamovich *et al.*, 2023). Notably, these

researchers were not able to record mass spectra for these materials and cited hydrolytic instability as the major issue.

However, it is noted that the spectrum of BPPrAsil-Pb + NaI at 0.1 M NaOH produced a base peak at an M/Z of 263, which was not present in the spectra of the non-metallated silicas, for which in both cases, the base peak was at M/Z 364. This peak is still present in the spectrum of BPPrAsil-Pb + NaI at 1 M NaOH, but is greatly reduced in abundance (Fig. S3). As such, it is possible that this ion could represent an iodide-loaded species.

The UV–vis spectra of the samples revealed a peak at  $\sim 260$  nm, which is known to correspond to the BPA moiety (Wang et al., 2009). We observed a similar peak when M4195 resin samples were leached with methanol (Robshaw et al., 2020). For samples run at pH 13 only, an additional strong peak appears at 214 nm, which it is thought represents the iodide-bearing complex. Interestingly, this peak was present for the BPPrAsil sample, as well as the BPPrA-Pb sample, which indicates the solubilised complex does not include a Pb ion. A similar peak was observed in the spectrum of PbNO<sub>3</sub>, but upon close inspection, this peak has a lower  $\lambda_{max}$  and the similarities are superficial (Fig. S4).

Overall, while inconclusive, the results strongly suggest the hydrolysis products are different at the two different pHs and that this is significant to iodide binding. The presence of colloidal silica species in downstream effluent, caused by partial hydrolysis of the adsorbent in base, would be of concern in practice (Sole et al., 2018), but especially if this led to radioiodine leaching from the column. These adsorbent materials were selected with a 'once through' system in mind, meaning the spent adsorbent column would be taken offline and processed as active waste. Most adsorbents are designed to be recyclable and operate over many cycles of use. From this perspective, both adsorbents would be problematic, because of the level of Pb leaching across the pH range. This would gradually change the uptake behaviour over many cycles and lead to a weaker ion-exchange mechanism becoming the dominant iodide removal process. The exception would be BPPrAsil-Pb at pH 8-12 (Fig. 2(b)), although the amount of iodide removal is probably too low for this attribute to be of practical use.

It should be noted that all subsequent uptake experiments were conducted without any pH control. The pH of iodide-containing solutions, post-adsorbent contact, was checked in these experiments. The pH value was observed to be  $\sim$ 5.5 in the case of M4195-Pb, and  $\sim$ 6.8 in the case of BPPrAsil-Pb.

#### 3.3.2. Isotherms

Fig. 3(a) shows iodide loading isotherms for the two adsorbents. The five models used have been previously employed to investigate sorbent uptake characteristics of iodide and other halides (Robshaw et al., 2019; Barton et al., 2019). Table S7 shows key isotherm model parameters. For the Redlich-Peterson model, modelling returned low  $\rm R^2$  values ( $\sim\!0.9$ ) and uncertainty values for calculated parameters were greater than the parameters themselves, rendering the data meaningless. Therefore data are not presented. This implies that a hybrid chemisorption/physisorption model is not applicable because the two mechanisms are metal complex formation and ion-exchange (not multilayer physisorption).

The  $q_{max}$  values for M4195-Pb and BPPrAsil-Pb were determined from the Langmuir isotherm to be  $338\pm12$  and  $46.5\pm7.6$  mg g<sup>-1</sup> respectively. The maximum uptake capacity,  $q_D$ , was also determined from the D-R isotherm as  $762\pm62$  and  $181.8\pm49$  mg g<sup>-1</sup> for M4195-Pb and BPPrAsil-Pb. Langmuir R<sup>2</sup> values were however rather higher and are taken as more valid. The Langmuir isotherm gave the best description of M4195-Pb data (R<sup>2</sup> = 0.993), but in fact, the Temkin isotherm gave the best fit for BPPrAsil-Pb (R<sup>2</sup> = 0.966). This is perhaps significant, as it suggests that the adsorption process could be influenced by indirect adsorbate/adsorbate interactions (Bezzina et al., 2020). The Langmuir isotherm describes monolayer adsorption with degenerate binding sites and homogeneity of the adsorption energy. This is clearly erroneous in the case of M4195-Pb, as the quantity of iodide adsorbed at higher  $C_i$  values is far in excess of what would be possible by ligation to

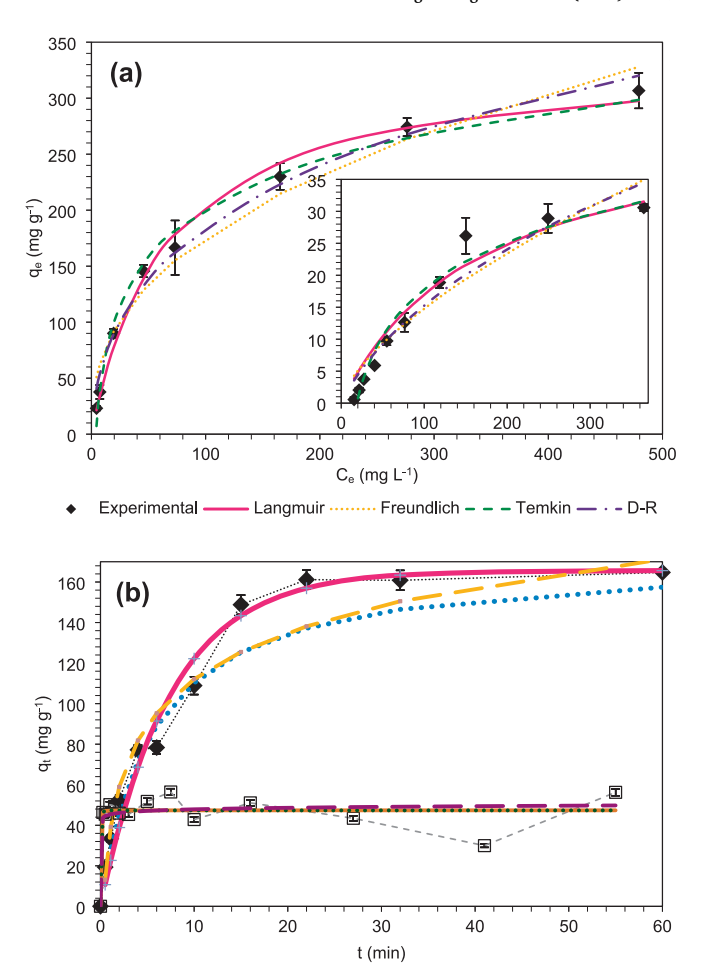


**Fig. 3.** (a) Iodide loading isotherms for M4195-Pb and (inset) BPPrAsil-Pb, with associated model-fitting. Adsorbent mass =50 mg. Solution volume =25 mL.  $T=20\,^{\circ}\text{C.}$   $C_i=(M4195\text{-Pb})$  50–1000 mg  $L^{-1},$  (BPPrAsil-Pb) 20–300 mg  $L^{-1}.$  (b) Iodide uptake over time for M4195-Pb and BPPrAsil-Pb, with associated model-fitting. Adsorbent mass =200 mg. Solution volume =1000 mL.  $C_i=1000$  mg  $L^{-1}.$   $T=20\,^{\circ}\text{C.}$ 

····• Experimental (M4195-Pb)

- - - Experimental (BPPrAsil-Pb)

PFO (M4195-Pb)

· · · · PFO (BPPrAsil-Pb)

•••• PSO (M4195-Pb)

Elovich (M4195-Pb)

- PSO (BPPrAsil-Pb)

- Elovich (BPPrAsil-Pb)

the Pb ions only, and must indicate interaction of the iodide with protonated ammoniums (Table 1). The Langmuir model has previously been able to model a system dominated by physisorption (Robshaw et al., 2019) and this does not necessarily imply the fundamental assumptions of the model are validated. The  $K_L$  parameter from the Langmuir isotherm however is useful in showing how strongly the adsorbent interacts with the iodide. M4195-Pb returned a  $K_L$  value of 0.0152  $\pm$  0.0017 and the BPPrAsil-Pb 0.00577  $\pm$  0.0019; an order of magnitude difference binding strength.

The Freundlich isotherm had the worst fit for both compounds with a value of  $R^2$  of 0.964 and 0.895 for M4195-Pb and BPPrAsil-Pb respectively. This isotherm best fits multi-layer adsorption processes and since both adsorbents work by ion-exchange, this is to be expected. The silica data were actually described best by the Temkin isotherm, which has previously been observed in studies where there are multiple non-degenerate sorbent/sorbate surface interactions (Robshaw et al., 2020). This fits with the proposed uptake chemistry.

The  $E_{des}$  value determined from the D-R isotherm indicates the strength of adsorption occurring and for M4195-Pb was found to be 7.74  $\pm$  0.8. This is likely a cumulative value, given the relatively low degree

of Pb loading. The adsorption, particularly at higher iodide concentration, will be dominated by anion-exchange and association with the numerous protonated nitrogens in the BPA functionality, that are not coordinating Pb ions. The equivalent for BPPrAsil-Pb was  $9.15\pm0.6,$  which is regarded with some scepticism because of the low  $R^2$  value of 0.919. It was clear from the addition of cocontaminants (Section 3.2.4) that the interaction of iodide with BPPrAsil-Pb is weaker, due to the silica matrix impact. The Langmuir separation factor  $(R_L)$  is likely a more accurate representation of binding strength (since the data fit the Langmuir model better).

We plotted  $R_L$  against iodide  $C_i$  for both adsorbents (Fig. S5).  $R_L$  increased for both materials with  $C_i$ , showing increasingly favourable adsorption. This illustrates the impact of the non-metal-loaded BPA groups on the adsorption overall, as this behaviour is more suggestive of an ion-exchange interaction (being affected by the ion concentration gradient) than metal complex formation. However, the change in  $R_L$  was much greater over the concentration range studied for the silica. The likely explanation is that at low  $C_i$ , the iodide in solution promotes leaching of singly-chelated  $Pb^{2+}$  ions and forms  $PbI_3^-$  and  $PbI_4^{2-}$  aqueous complexes (Lanford and Kiehl, 1941; Stevenson et al., 2017), producing  $R_L$  values close to 1 (unfavourable adsorption). As  $C_i$  increases, binding to the adsorbent occurs via the doubly-chelated  $Pb^{2+}$  ions. XPS data provided strong evidence for this (Section 3.4).

As a general point, a key parameter for these adsorbents would be the 'efficiency' of iodide-loading achieved, with respect to the number of iodide anions ligated per Pb cation. However, this is not possible to calculate in this instance, because of the relatively low-level of Pb-loading achieved and the competing anion-exchange mechanism with both coordinated and uncoordinated BPA groups. Clearly, the selection of both chelating ligand and loading metal is of great importance to secure maximal metal loading and minimise the weaker ion-exchange interactions, since these are deleterious to wasteform performance (Simoni et al., 2024).

The reported capacity of metalated adsorbents for iodine species is highly variable (13->400 mg g<sup>-1</sup>) and the reader is directed to a recent review for comparison (Robshaw et al., 2021). Iodide capacity is generally not dependent on choice of loading metal. For example, an Agloaded titanate has been shown to adsorb 430 mg iodide g<sup>-1</sup> (Bo et al., 2013), while an Ag-functionalised synthetic zeolite adsorbs only 20 mg g<sup>-1</sup> (Tauanov and Inglezakis, 2019). The Pb-loaded M4195 resin has a higher theoretical iodide capacity than the equivalent Cu-loaded M4195 from previous work, for which the Langmuir-calculated q<sub>e</sub> was 300 mg  $g^{-1}$  (Robshaw et al., 2020). However, this is likely because the lower Pb metal-loading allows more iodide to be loaded by weaker ion-exchange interactions. The choice of adsorbent matrix physicochemistry is instrumental in dictating the density of possible metal binding sites and the chemical form of the metal on the adsorbent surface (salt, nanoparticle or ligated ions) (Robshaw et al., 2021). This issue has very much prompted current investigations.

## 3.3.3. Kinetic experiments

Kinetic data between the two adsorbent matrices are also radically different (Fig. 3(b), Table S8). Adsorption for M4195-Pb reaches equilibrium fairly steadily over ~20 mins. Although the higher  $R^2$  value suggested good agreement to the Pseudo-First-Order (PFO) model, the data failed the test for non-randomness (Revellame et al., 2020). As such, the adsorption rate is dependent on neither ( $\theta_e - \theta_t$ ), nor ( $\theta_e - \theta_t$ )<sup>2</sup> entirely, which possibly indicates hybrid kinetics (Liu and Shen, 2008) ( $\theta_e$  = equilibrium adsorption site coverage,  $\theta_t$  = adsorption site coverage at time t). The simplified Elovich equation also did not describe the data well, which is perhaps surprising, as it has sometimes been shown to describe a heterogeneous system well, where different rate constants are rate-controlling at different times (Robshaw et al., 2019). Compared to iodide uptake by previously-reported metal-loaded or —based adsorbents, equilibrium is rapid. A BiPbO<sub>2</sub>(NO<sub>3</sub>) material required ~10 hr to reach equilibrium (Kodama, 1999). An Ag-loaded ion-exchange resin

was more similar in performance, reaching  $\sim 90$  % equilibrium capacity in 30 min (Decamp and Happel, 2013).

For BPPrAsil-Pb, the system clearly reaches ~ 100 % equilibrium uptake almost instantly. However, the iodide solution concentration then fluctuated greatly, meaning that no model gave a precise fit to the data. This again speaks to the instability of the system, as it is clearly far more sensitive to small variations in temperature, pressure and change in solution volume. While the BPPrAsil-Pb adsorption is seemingly weak, it is exceptionally rapid, reaching  $> 40 \text{ mg g}^{-1}$  in < 0.5 min, which is unlike any metalated adsorbent yet reported (Robshaw et al., 2021). Nor is this behaviour typical for a functionalised silica. It has been observed that the adsorption of Sr<sup>2+</sup> by ethyl/butyl phosphonate silica takes ~ 60 min to reach near equilibrium (Pepper et al., 2024). For context, the BPPrA silica was loaded with Cu<sup>2+</sup> ions, in a similar procedure to that mentioned in the Experimental section. The data are not presented here, but it was found that uptake was similarly rapid. Therefore, the behaviour is attributed to the physicochemical properties of this particular silica. It is possibly a consequence of only surface bromo groups being converted to BPA groups, as predicted from Table 1, meaning that there are no instances of iodide anions having to diffuse through the mesopore network to internal adsorption sites (though as noted, there is no satisfactory explanation as to why the internal sites were not successfully functionalised).

#### 3.3.4. Iodide uptake in competitive conditions with co-anions

The introduction of relevant competing anions to the system had varying effects upon the two systems (Figs. S6 and S7). The M4195-Pb retained reasonable iodide uptake performance in the presence of both an outer-sphere anion (nitrate) and a chelating inner-sphere ligand (molybdate), even at high ionic strength; with iodide K<sub>D</sub> values not changing significantly (Table S9). In contrast, the BPPrAsil-Pb retained some selectivity in the nitrate system, but any molybdate reduced the iodide adsorption to below detectable levels. Certainly, there is sufficient evidence throughout this paper that the binding of iodide ligands to Pb ions is destabilised in the silica matrix; but presumably, this would also apply to competing ligands. We believe the explanation is that doubly-coordinated "bridging" Pb ions would be more selective towards iodide than molybdate, as the molybdate would chelate through two oxygen atoms and therefore require two coordination sites (Rarig et al., 2002), which would be sterically difficult with a Pb ion already bound to two BPA moieties. This behaviour is feasible in a crowded pore network, but much less likely with the silica, since the evidence all suggests it is functionalised only on the particle surface, rather than within the mesopores. For singly-chelated Pb ions, the laws of complex stability would likely dominate and therefore molybdate would strongly suppress iodide uptake (PbI $_2$  K $_{sp} = 4.4$  x  $10^{-9}$ , PbMoO $_4$  K $_{sp} = 1.2 \pm 0.3 \times 10^{-13}$  (Chao and Cheng, 1977).

Compared to a Cu-loaded M4195 resin in similar experimental conditions, M4195-Pb had  $\sim75~\%$  retention of iodide uptake at high nitrate and molybdate concentrations, verses  $\sim55~\%$  (Robshaw et al., 2020). However, in terms of iodide selectivity in aggressive chemical conditions, predictably, neither adsorbent can compete with Ag-loaded materials, because of lower soft acid/base affinity (Robshaw et al., 2022; Asmussen et al., 2023).

## 3.4. Solid-state characterisation of materials at various processing stages

Fig. 4 shows the  $N_2$  adsorption/desorption isotherms attained for the materials studied. The calculated pore size distributions for each material are seen in Fig. S8. The silica materials all demonstrated Type IV isotherms with H1 hysteresis loops, which is typical behaviour for mesoporous solids and indicates cylindrical pore geometry and narrow distribution of pore size (Sing, 1982). The resin samples give a Type III isotherm, suggesting unrestricted multilayer formation, due to the large volume of the macropores. It is accepted that gas adsorption is not the preferred technique for macropore analysis and the results for M4195

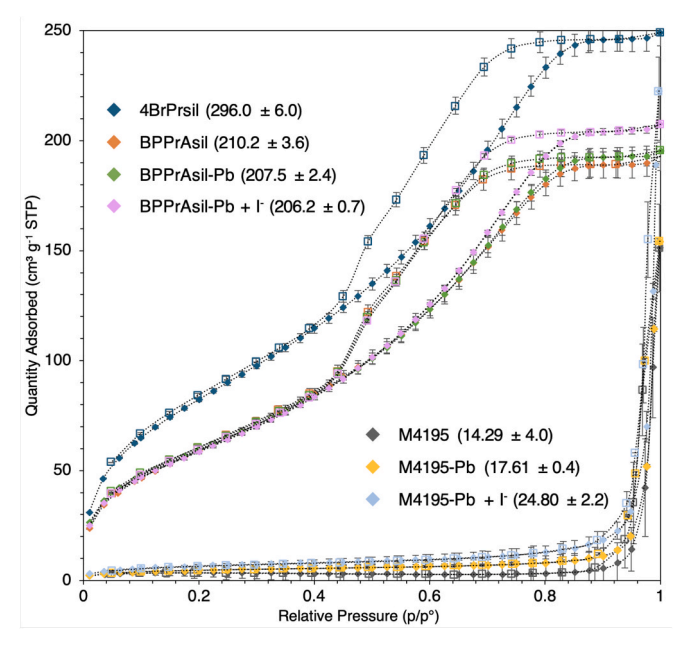


Fig. 4.  $N_2$  Adsorption/desorption isotherms of the materials studied (Diamonds show adsorption, squares show desorption datapoints). Total BET calculated surface areas are shown in  $m^2$   $g^{-1}$ .

samples are only presented as comparisons to the silicas, in terms of the effects of metal and iodide addition. Interestingly though, the further addition of  $Pb^{2+}$  ions and large iodide ligands to the system did not result in significantly less surface area. In fact, the measured surface areas were almost equivalent, within the margin of experimental uncertainty (Fig. 4). This is in contrast to previous work on metalation of porous adsorbents, in which the addition of metal ions decreased measurable surface area (indeed the degree of decrease was even proportionate to the size of the metal ion) (Robshaw et al., 2020; Ma et al., 2014). In our work, this might be due to simply the low degree of metal and iodide loading achieved. However, it may also be due to the Pb2+ cation being too large to fit within the plane of the BPA cavity (Diniz et al., 2002). This would essentially create inefficient "packing" at the molecular scale and create more sites for the small gas molecules to adsorb (McKeown, 2017). Iodide anions do not actually occupy that much more volume than the nitrate ions they displace upon adsorption (ionic radii = 206 and 132 pm), which may also explain the minimal effect on surface area. The M4195 samples appear to increase in porosity upon binding of both Pb and iodide. This is tentative because of the limitations of N<sub>2</sub> adsorption in modelling macroporous materials. However, ion-exchange resins are widely known to swell in water, upon introduction of larger ions.

The main objective of acquiring XRD data was to check for crystallisation of Pb species, which could affect the uptake of iodide. The M4195-Pb samples showed a surprising prevalence of such crystalline species across the adsorption pH range (Fig. S9), with basic lead carbonate ( $C_2H_2O_8Pb_3$ ,  $K_{sp}=1.46\times10^{-13}$ ) and lead sulfate (PbSO<sub>4</sub>,  $K_{sp}=$  $2.13 \times 10^{-8}$ ) being detectable in all samples, though in much higher quantities at pH 9 and above. The sulfate would have been present in the samples, as it is involved in the manufacture of M4195 and difficult to remove, even through repeated resin conditioning (Robshaw et al., 2020). Quantification of these species was not possible, as the spectra were mainly amorphous and so could not be subjected to the relevant analysis. XPS analysis of a sample collected at neutral pH (Fig. 5(b)) did not detect any crystalline species. The formation of these salts was clearly a competing mechanism to the uptake of iodide (Fig. 2), and might represent a barrier to the use of M4195-Pb in basic conditions, at least without control of CO2 contamination). Other species observed were  $PbO(\alpha)$  and  $PbO(\beta)$ . It has been reported that precipitation of both

species from  $Pb(NO_3)_2$  solutions is possible in the presence of a low concentration of chloride ions (Cheng et al., 2010) and it is presumed that the iodide in our experiments could have functioned in the same way.

The BPPrAsil-Pb diffractograms were all featureless below pH 6, but did also reveal some  $C_2H_2O_8Pb_3$  at more alkaline pHs (samples could not be collected beyond pH 11 because of dissolution). Overall, the Pbloaded adsorbents were more prone to crystallisation of undesirable species than the Cu-loaded equivalent (Robshaw et al., 2020).

The XPS surface atomic composition sweep scans confirm that most BPA functionalisation is on the surface of the silica particles. XPS is a surface-sensitive technique and the recorded atomic mass % for carbon is close to that of silica (Table S10), whereas the elemental analysis demonstrates the composition of the silica materials was <10 % carbon mass in total (Table 1). Notably, the scans of M4195-Pb samples showed a much lesser Pb concentration that would be expected, relative to N. The lowest atomic ratio expected would be  $\sim$ 1:8, as this would represent a Pb<sup>2+</sup> ion chelated to two BPA ligands, with two nitrate counteranions; whereas the actual ratio is  $\sim$ 1:30–1:50 (Table S10). This is again incongruous with Table 1 and we must assume there is a disparity between the surface sites and pore interior sites for M4195.

The high resolution N 1s scans for M4195 and BPPrAsil revealed a most interesting difference between the matrices. Three N environments were observed in both cases, representing (in order of increasing binding energy) neutral amines, protonated/quaternised amines, and nitrate ions (Robshaw et al., 2020; Song et al., 2012). However, the binding energies for the silica samples were consistently higher than for the resin samples. We believe this represents the postulated extensive hydrogen bonding between the BPA nitrogens and surface silanol groups, which would account for the weaker Pb binding observed and tendency for Pb leaching (Fig. 2). Song et al. reported that hydrogen-bonding of amine groups generally increases the N 1s binding energy, though by quite a variable amount (0-1.5 eV), depending on the H-bonding partner (Song et al., 2012). For clarity, it should be noted that a protonated ammonium nitrogen is still capable of being a H-bond acceptor (Song et al., 2012; Nieto et al., 2017). We were not able to locate any specific XPS studies which characterised the effects of H-bonding on the N 1s spectrum for nitrate ions. This conclusion is tentative because as noted in SI (p6), instrument calibration could not be performed by fixing the main C 1s peak at 285 eV, as is conventional (because of the noisy carbon spectra attained). Therefore, the nitrogen peak shifts between resin and silica samples may be due to systematic bias from the instrument. It should be noted though that there is no evidence of this possible systematic bias with respect to other elements, including Pb (Fig. 5(b)).

The N 1s scans also demonstrate the relative weakness of interaction between the BPA group and the coordinated Pb ions, as there is no significant change in N 1s binding energy between the free amine and Pb-loaded samples (Table S12). This is in contrast to XPS spectra attained for the M4195 resin loaded with  $\text{Cu}^{2+}$  ions, where there was a shift of  $+{\sim}0.5$  eV upon Cu coordination (Robshaw et al., 2020). This would explain the tendency for Pb to leach during iodide uptake, especially in the case of the silica.

The high-resolution Pb 4f scans (Fig. 5(b)) show only a single Pb environment for both resin and silica samples, both before and after iodide contact, with the Pb in 2 + oxidation state throughout (Olthof and Meerholz, 2017). This is dissimilar to spectra acquired for Cu-loaded adsorbent, in which the different binding environments for singly- and doubly-chelated metal ions were clearly distinguished (Robshaw et al., 2020). This suggests that the great majority of Pb ions present were doubly-chelated. It is likely that the singly-chelated species were volatilised, which would explain the low atomic abundance compared to Table 1. No crystalline Pb species, observed in XRD spectra were detected, which implies they were present at very low concentrations and/or mainly formed in the pores of the materials, where there was more accessible surface area for nucleation sites (Robshaw et al., 2020). Upon iodide-coordination, the Pb environment for both materials shifts

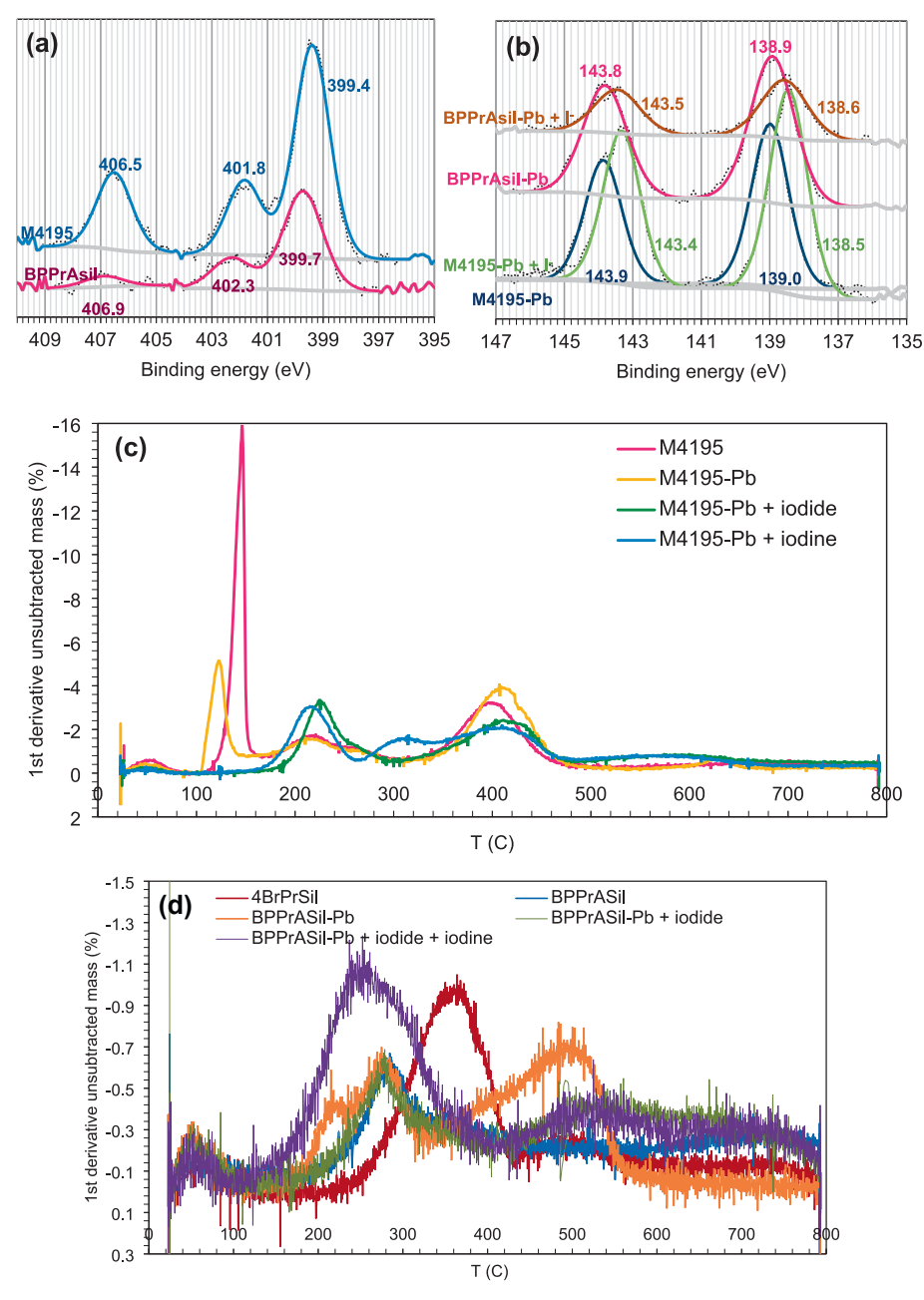


Fig. 5. Chemical analysis of resin and silica samples at various processing stages. (a) XPS high-resolution N 1s scans for M4195 (top) and BPPrAsil (bottom). (b) XPS high-resolution Pb 4f scans for Pb-loaded adsorbents before and after iodide-contact: BPPrAsil-Pb (top) and M4195-Pb (bottom). (c) and (d) First derivative TGA traces for resin (top) and silica (bottom) samples.

to a lower binding energy, which is consistent with more favourable electron density donation from the softer iodide ligands. The values for the 7/2 spin orbital coupling of 138.5 and 138.6 are in excellent agreement with those recorded by Olthof and Meerholz for a MAPbI<sub>3</sub> perovskite (Olthof and Meerholz, 2017). This suggests that the BPA ligand has only a slight effect on the electronic properties of the coordinated Pb<sup>2+</sup> ions, again implying a surprisingly weak interaction. It should be noted that the binding energy change, upon iodide-coordination, is lesser for BPPrAsil-Pb than for M4195-Pb (0.3 eV vs 0.5 eV). This may indicate that the hydrophilic matrix destabilises the Pb-I bonding, as well as the Pb-N bonding. It is well known through study of conventional IX resins that the lower the crosslinking degree (and therefore the hydrophibic ions (Harland, 1994). However, this literature relates to pure ion-exchange interactions rather than ligand-

exchange. It is arguable whether the observed differences in binding energies are significant enough to draw this conclusion.

# 3.5. Thermal degradation profiles of the materials at various process stages

TGA data are especially relevant for these adsorbents, because various routes of processing of active waste involve elevated temperatures (Atkinson et al., 2025) and weakly-bound iodine, that does not convert to a stable metal salt at high temperature, will lead to volatilisation and potential loss to the atmosphere. The TGA traces (Fig. 5(c) and (d)) yet again revealed interesting differences in how the different adsorbents degraded at a function of temperature. For clarity, the individual first derivatives for the silica samples are shown in the SI, Fig. S12.

The non-iodine-loaded resin samples initially lost the numerous associated nitrate counterions at  $\sim$  120–160  $^{\circ}\text{C}.$  This is much lower than the reported 1st decomposition of e.g Pb(NO<sub>3</sub>)2 (Nair et al., 1984). However, it is noted that an M4195 sample with sulfate counteranions did not exhibit a mass loss at this temperature (Robshaw et al., 2020). The samples then exhibited a pattern fairly typical of anion-exchange resins (Yang et al., 2014; Dubois et al., 1995), with the BPA functionality being lost at  $\sim$  220  $^{\circ}$ C and the styrene/divinylbenzene matrix at  $\sim$ 400  $^{\circ}$ C. It is known that PbO decomposition occurs in multiple stages in the range 330-570 °C (Gavrichev et al., 2008) and this can also be observed in the relevant resin and silica thermograms. PbI2 decomposes between 425 and 600 °C (Ren et al., 2017) and therefore the distinctions between iodine- and non-iodine-loaded samples at this range are not particularly clear. Notably, the decomposition of the BPA group for the silica sample appeared to take place at a rather higher temperature than for the resins, beginning at  $\sim 290$  °C. We believe this is correlated to the extent of H-bonding between the ligand and surface silanol groups; stabilising the ligand. Also interesting is that molecular iodine appears to be adsorbed rather more stably in the resin sample, as it decomposes at >300 °C (consistent with literature values (Luca et al., 2017) vs  $\sim$ 250 °C. This can again be attributed to matrix differences, as the molecular iodine would form stable charge-transfer complexes with the aromatic rings of M4195 (Robshaw et al., 2020), whereas in the silica sample, it would only weakly associate with the alkyl remnants of the ligands (these appear to decompose at  $\sim 500\,^{\circ}$ C). One clear advantage of both adsorbents over the previously-studied Cu-loaded M4195 resin is that there is no evidence in TGA data (or any other analysis performed)

of in-situ oxidation of iodide to more lipophilic and volatile species. In both sets of thermograms, there is no evidence of  $\rm I_2$  mass loss unless samples are actually treated with  $\rm I_2$ . However, the issue of iodide adsorbing by ion-exchange to non-metallated BPA groups is clear, as it decomposes alongside the ligand. This is seen most clearly in Fig. 5(c) at  $\sim 220{-}230~^{\circ}\text{C}$ .

# 3.6. Future elucidation of H-bonding interaction between surface silanol groups and the BPA ligand

This paper has proposed a H-bonding interaction (Fig. 6), unique to the silica matrix, to be the main cause of the variations in uptake behaviour observed between the two matrices. Producing incontrovertible proof of this interaction will be a difficult task. Normally FT-IR would be useful, as it can in some circumstances distinguish between H-bonded and non-H-bonded amines. However, as we observed (Fig. S2), this is not possible for silica-based samples, because the FT-IR cannot detect the organic component of the sample.

We attempted to further elucidate the interaction by acquiring solidstate <sup>1</sup>H-<sup>15</sup>N CP MAS NMR spectra of resin and silica samples at the UK 850 MHz Facility (University of Warwick). However these experiments were unsuccessful, because even the high-field instrument could not produce a sufficient signal-to-noise ratio to produce clear peaks for the N environments. Therefore these data are not presented. This demonstrates some of the difficulties in qualifying these interactions in challenging sample matrices.

One possible route forward would be to synthesise a small organic

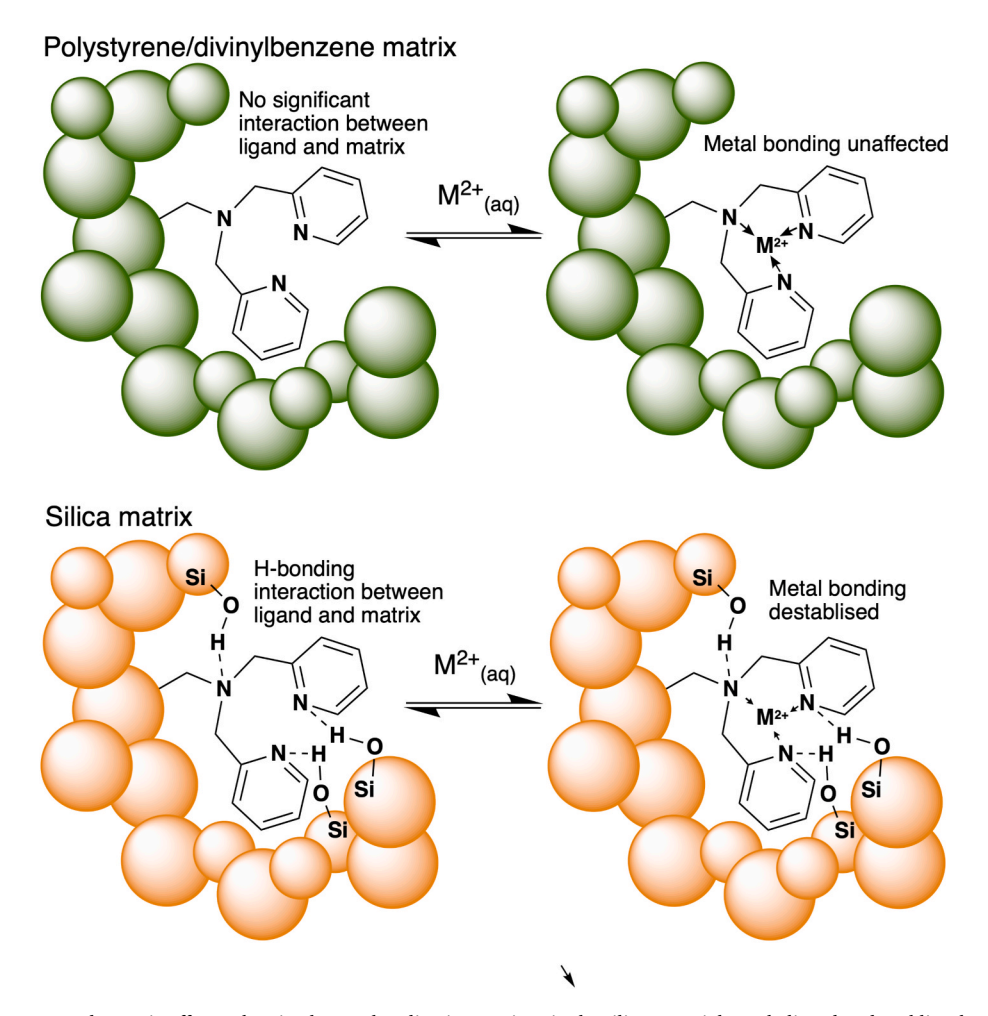


**Fig. 6.** Illustration of the proposed "matrix effect", showing how H-bonding interactions in the silica materials are believed to destablise the metal ion binding to the BPA functionality. Shaded spheres represent the matrix/pore environment of each adsorbent.

molecule containing both BPA and silanol functionalities (Lickliss and Sykes, 1995). It would then be possible to probe the inter- and intramolecular H-bonding with standard NMR techniques (although this would not of course prove definitively that such interactions occur between ligand and solid silica surface). Such investigations are beyond the scope of the current work, but are targeted for the future.

#### 3.7. Observations on industrial applicability of the systems studied

In general, the experiments conducted have demonstrated that the different adsorbent matrices used impart remarkable influence on the adsorption properties; even when the same chemical functionality and loading metal are employed.

As mentioned, the Pb/BPA functionality has the advantage of not converting the adsorbed iodide to higher and more volatile oxidation states, unlike the previously-assessed Cu/BPA. Unfortunately however, the large size of the Pb<sup>2+</sup> cation results in the bridging interactions between multiple BPA groups, and many uncoordinated amine sites This is not detrimental to ultimate capacity for iodide, because of the anion-exchange behaviour of uncoordinated BPA groups. However, this weak iodide adsorption is very problematic when the loaded materials are encapsulated in cement for GDF disposal, as a large fraction of the iodide is readily leached (Kearney et al., 2022; Simoni et al., 2024). Thermal treatments of (both) materials for waste conversion would also be problematic, as the radioiodine, even when adsorbed entirely as iodide, would readily volatilise under vitrification, or even oxidation (Bingham et al., 2012).

M4195 is overall the more feasible adsorbent for the intended process, being able to load significantly more Pb ions, and also to retain metal-loading and physical stability in harsher chemical conditions. BPPrAsil-Pb possesses faster uptake kinetics, but in all other pertinent adsorption parameters, it is inferior.

Another important consideration is radiolytic stability of the adsorbents. Previous literature on the radiolytic breakdown of IX resins has shown that the heteroatom functionality (rather than the styrene matrix) is the first part of a resin to degrade (Bartonicek et al., 1983). SiO2 is of course immune to radiolytic attack. Therefore, a most interesting question is whether the matrix effects seen throughout this investigation would play a part in the stability of the BPA moiety under radiolysis. This is important future work. The silica matrix has cement wasteform compatibility, notwithstanding the issue of leaching (Simoni et al., 2024; Robshaw et al., 2023). However, IX resins are also amenable to several processing routes including vitrification, cementation and plastic solidification (Atkinson et al., 2025). This study demonstrates the necessity of holistic considerations of adsorbent design, as it seems the BPA ligand is fundamentally poorly-compatible with the silica matrix, because of the destabilising H-bonding likely occurring. This is not the case for all organosilicas; for example, it has been shown that an Agloaded mercapto group (non H-bonding) has extremely strong affinity for iodide (Robshaw et al., 2023).

For highly targeted separation processes, there is a need for control of adsorption properties at the molecular scale. In this case, the ideal adsorbent would be designed such that all iodide adsorbed would do so as metal ligands, rather than weaker ion-exchange. Otherwise the fundamental capacity advantage of chelated metal ions over e.g. precipitated nanoparticles or metal salts (Robshaw et al., 2021) is negated.

## 4. Conclusions

We have comprehensively compared two different adsorbent materials for the removal of iodide from aqueous solutions, with a view to remediation and safe containment of iodine-129 in nuclear fuel recycling. While sharing the same chemical functionality of Pb-loaded bispicolylamine (BPA), one adsorbent was a polymeric resin (M4195-Pb) and the other a functionalised organosilica (BPPrAsil-Pb). The

differences in fundamental uptake and retention behaviour were stark and illustrated that matrix chemistry must be very carefully considered in liquid/solid separation processes. For both materials, Pb loading was low, relative to BPA group concentration, which suggested the Pb<sup>2+</sup> ions bridge across multiple groups. Pseudo-pKa values were determined, which illustrated that the BPPrAsil matrix caused acidification of the amine groups. This correlated to relatively high Pb-leaching at mildly acidic pH, compared to M4195-Pb. The resin demonstrated higher theoretical maximal iodide loading of 338  $\pm$  12 mg g<sup>-1</sup>, compared to  $46.5 \pm 7.6 \text{ mg g}^{-1}$  (calculated by the Langmuir model), in line with its greater functional group-loading. It also retained iodide-capture more strongly, in the presence of cocontaminants. However, the silica had extremely rapid uptake kinetics, with near maximal (though unstable) iodide-loading attained within 1 min, which suggested it was functionalised only at the particle surface rather than within the pores. Spectroscopic investigations further evidenced that Pb-loading was significantly destabilised for BPPrAsil, causing the observed leaching; the most likely explanation being that the BPA ligand forms extensive Hbonds with surface silanol groups. Quantifying the degree of surface charge of the two materials over a pH range is clearly of relevance for further elucidation of the differences in iodide-binding behaviour and such investigations are ongoing. In terms of thermal stability, it was found that molecular iodine was volatilised at lower temperatures for the silica, but iodide itself was more stably bound, probably because of the H-bonded ligand's enhanced thermal stability. While there are issues with potential deployment of either material for the remit of radioiodine treatment, this study highlights some of the complexities around rational adsorbent selection; both for this remit and broader. It is hoped it will progress the agenda to advance adsorbent manufacture from reliance on petrochemical feedstocks.

#### CRediT authorship contribution statement

Thomas J. Robshaw: Writing - review & editing, Writing - original draft, Validation, Supervision, Project administration, Methodology, Investigation, Funding acquisition, Formal analysis, Data curation, Conceptualization. Fiona M. Lambert: Writing - original draft, Methodology, Investigation, Formal analysis. Sophie D. Watson: Writing original draft, Methodology, Investigation, Formal analysis, Data curation. Supakorn Tantisryanurak: Methodology, Formal analysis. Nuha Mukhtar: Formal analysis, Data curation. Victoria Shields: Supervision, Investigation, Formal analysis, Data curation. Joshua Turner: Writing - review & editing, Supervision, Resources, Project administration, Funding acquisition, Conceptualization. Robert Dawson: Supervision, Software, Resources. Brant Walkley: Writing - review & editing, Supervision, Investigation, Funding acquisition, Conceptualization. Clint A. Sharrad: Supervision, Resources, Project administration, Funding acquisition, Conceptualization. Mark D. Ogden: Writing review & editing, Supervision, Resources, Project administration, Funding acquisition, Conceptualization.

#### **Declaration of competing interest**

The authors declare that they have no known competing financial interests or personal relationships that could have appeared to influence the work reported in this paper.

#### Acknowledgements

We would like to thank Dr Deborah Hammond, of the Sheffield Surface Analysis Centre (SSAC), for running the XPS instrument. We also acknowledge Dr Dinu Iuga, of the University of Warwick 850MHz NMR Facility, for his efforts in attempted high-field  $^1\mathrm{H}\text{-}^{15}\mathrm{N}$  CP MAS experiments.

#### Funding

This research was partially funded under the £46 m Advanced Fuel Cycle Programme as part of the Department for Business, Energy and Industrial Strategy's (BEIS) £505 m Energy Innovation Programme.

#### Appendix A. Supplementary data

Supplementary data to this article can be found online at  $\frac{\text{https:}}{\text{doi.}}$  org/10.1016/j.ces.2025.122799.

#### Data availability

Data will be made available on request.

#### References

- Alexandratos, S.D., 2009. Ion-exchange resins: a retrospective from industrial and engineering chemistry research. Ind. Eng. Chem. Res. 48 (1), 388–398. https://doi.org/10.1021/je801249v
- Chiarizia, R., Horwitz, E.P., Beauvais, R.A., Alexandratos, S.D., 1998. Diphonix-CS: a novel combined cesium and strontium selective ion exchange resin. Solv. Extr. Ion Exch. 16 (3), 875–898. https://doi.org/10.1080/07366299808934558.
- Wilson, H., Byrne, S., Bampos, N., Mullen, K., 2013. 'Click' functionalised polymer resins: a new approach to the synthesis of surface attached bipyridinium and naphthalene diimide [2]rotaxanes. Org. Biomol. Chem. 11, 2105–2115. https://doi. org/10.1039/c3ob27273g.
- Robshaw, T., Tukra, S., Hammond, D.B., Leggett, G.J., Ogden, M.D., 2019. Highly efficient fluoride extraction from simulant leachate of spent potlining via La-loaded chelating resin. an equilibrium study. J. Haz. Mat. 361, 200–209.
- Bezzina, J.P., Ogden, M.D., Moon, E.M., Soldenhoff, K.L., 2018. REE behavior and sorption on weak acid resins from buffered media. J. Ind. Eng. Chem. 59, 440–455. https://doi.org/10.1016/j.jiec.2017.11.005.
- Shields, V.R., Robshaw, T.J., Amphlett, J.T.M., Porter, C.P., Hides, A., Bruce, R., Cordiner, J., Ogden, M.D., 2023. Gold recovery from simulant mine tailings using chelating ion exchange resins with thiosulfate-thiourea lixiviant. Resourc Conserv. Recycl. Adv. 19, 200182. https://doi.org/10.1016/j.rcradv.2023.200182.
- He, J., Yang, Y., Wu, Z., Xie, C., Zhang, K., Kong, L., Liu, J., 2020. Review of fluoride removal from water environment by adsorption. J. Env. Chem. Eng. 8. https://doi. org/10.1016/i.jece.2020.104516.
- Ni, C., Liu, C., Xie, Y., Xie, W., He, Z., Zhong, H., 2022. A critical review on adsorption and recovery of fluoride from wastewater by metal-based adsorbents. Environ. Sci. Pollut. Res. 29, 82740–82761. https://doi.org/10.1007/s11356-022-23416-8.
- Choe, J., Mehnert, M., Guest, J., Strathmann, T., Werth, C., 2013. Comparative assessment of the environmental sustainability of existing and emerging perchlorate treatment technologies for drinking water. Env. Sci. Tech. 47, 4644–4652. https:// doi.org/10.1021/es3042862.
- Amini, A., Kim, Y., Zhang, J., Boyer, T., Zhang, Q., 2015. Environmental and economic sustainability of ion exchange drinking water treatment for organics removal. J. Clean. Prod. 104, 413–421. https://doi.org/10.1016/j.jclepro.2015.05.056.
- C.M. Atkinson , G.D. Walker , T.J. Robshaw , M.J.D. Rushton , S.C. Middleburgh , M.D. Ogden, Optioneering in nuclear ion exchange resin disposal, Progr. Nucl. Energy 185. https://doi.org/10.1016/j.pnucene.2025.105719.
- Song, W., Gao, B., Guo, Y., Xu, X., Yue, Q., Ren, Z., 2017. Effective adsorption/desorption of perchlorate from water using corn stalk based modified magnetic biopolymer ion exchange resin. Micro. Meso. Mat. 252, 59–68. https://doi.org/10.1016/j. micromeso.2017.06.019.
- Zia, Z., Hartland, A., Mucalo, M., 2020. Use of low-cost biopolymers and biopolymeric composite systems for heavy metal removal from water. Inter. J. Envrion. Sci. Technol. 17, 4389–4406. https://doi.org/10.1007/s13762-020-02764-3.
- Tran, A., Pham, T., Nguyen, Q., Hoang, N., Bui, D., Nguyen, M., Nguyen, M., Van der Bruggen, B., 2020. From waste disposal to valuable material: Sulfonating polystyrene waste for heavy metal removal. J. Environ. Chem. Eng. 8. https://doi. org/10.1016/j.jece.2020.104302.
- Nuclear Energy Agency, State-of-the-art report on the progress of nuclear fuel cycle chemistry, Paris, 2018.
- Turner, J., 2021. Clean air, blue skies: capturing gases in a future advanced fuel cycle. Nucl. Fut. 17, 50.
- Robshaw, T.J., Turner, J., Kearney, S., Walkley, B., Sharrad, C.A., Ogden, M.D., 2021. Capture of aqueous radioiodine species by metallated adsorbents from wastestreams of the nuclear power industry: a review, SN. Appl. Sci. 3 (11). https://doi.org/ 10.1007/s42452-021-04818-8.
- Asmussen, R.M., Turner, J., Chong, S.H., Riley, B.J., 2022. Review of recent developments in iodine wasteform production. Front. Chem. 10. https://doi.org/ 10.3389/fchem.2022.1043653.
- Wang, J.L., Wan, Z., 2015. Treatment and disposal of spent radioactive ion-exchange resins produced in the nuclear industry. Progr. Nucl Energy 78, 47–55. https://doi. org/10.1016/j.pnucene.2014.08.003.
- Kearney, S., Robshaw, T.J., Turner, J., Sharrad, C.A., Walkley, B., Ogden, M.D., 2022. Encapsulation of iodine-loaded metallated silica materials by a geopolymer matrix. MRS Adv. 7 (5–6), 105–109. https://doi.org/10.1557/s43580-022-00207-4.

- Simoni, M., Kearney, S., Robshaw, T.J., O'Donoghue, K., Geddes, D., Sharrad, C.A., Ogden, M.D., Walkley, B., 2024. Encapsulation of iodine loaded adsorbents in blended Portland cement and geopolymer wasteforms. Cem. Concr. Res. 179, 107480. https://doi.org/10.1016/j.cemconres.2024.107480.
- Robshaw, T.J., Turner, J., Tuck, O., Pyke, C., Kearney, S., Simoni, M., Sharrad, C.A., Walkley, B., Ogden, M.D., 2022. Functionality screening to help design effective materials for radioiodine abatement. Front. Chem. 10. https://doi.org/10.3389/fchem.2022.997147
- Silva, R., Zhang, Y., Hawboldt, K., James, L., 2021. Study on iron-nickel separation using ion exchange resins with different functional groups for potential iron subproduction. Min. Proc. Extr. Metal. Rev. 42, 75–89. https://doi.org/10.1080/ 08827508.2019.1678155
- Aguila, B., Banerjee, D., Nie, Z.M., Shin, Y., Ma, S.Q., Thallapally, P.K., 2016. Selective removal of cesium and strontium using porous frameworks from high level nuclear waste. Chem. Commun. 52 (35), 5940–5942. https://doi.org/10.1039/c6cc00843g.
- James, A.M., Harding, S., Robshaw, T., Bramall, N., Ogden, M.D., Dawson, R., 2019. Selective environmental remediation of strontium and cesium using sulfonated hyper-cross-linked polymers (SHCPs). Appl Mat. Interf. 11, 22464–22473. https://doi.org/10.1021/acsami.9b06295.
- Robshaw, T.J., James, A.M., Hammond, D.B., Reynolds, J., Dawson, R., Ogden, M.D., 2020. Calcium-loaded hydrophilic hypercrosslinked polymers for extremely high defluoridation capacity via multiple uptake mechanisms. J. Mat. Chem. A 8, 7130–7144. https://doi.org/10.1039/C9TA12285K.
- Decamp, C., Happel, S., 2013. Utilization of a mixed-bed column for the removal of iodine from radioactive process waste solutions. J. Radioan. Nucl. Chem. 298 (2), 763–767. https://doi.org/10.1007/s10967-013-2503-1.
- Asmussen, R.M., Matyas, J., Qafoku, N.P., Kruger, A.A., 2019. Silver-functionalized silica aerogels and their application in the removal of iodine from aqueous environments. J. Haz. Mat. 379. https://doi.org/10.1016/j.jhazmat.2018.04.081.
- Barton, D.N.T., Robshaw, T.J., Okusanya, O., Kim, D., Pepper, S.E., Sharrad, C.A., Ogden, M.D., 2019. Remediation of radioiodine using polyamine anion exchange resins. J. Ind. Eng. Chem. 78, 210–221. https://doi.org/10.1016/j.jiec.2019.06.012.
- Hijazi, A., Azambre, B., Finqueneisel, G., Vibert, F., Blin, J., 2019. High iodine adsorption by polyethyleneimine impregnated nanosilica sorbents. Micro. Meso. Mat. 288. https://doi.org/10.1016/j.micromeso.2019.109586.
- Ye, Z.X., Chen, L.F., Liu, C.C., Ning, S.Y., Wang, X.P., Wei, Y.Z., 2019. The rapid removal of iodide from aqueous solutions using a silica-based ion-exchange resin. React. Funct. Polym. 135, 52–57. https://doi.org/10.1016/j.reactfunctpolym.2018.12.002.
- Asmussen, R., Ryan, J., Matyas, J., Crum, J., Reiser, J., Avalos, N., McElroy, E., Lawter, A., Canfield, N., 2019. Investigating the durability of iodine waste forms in dilute conditions. Materials 12 (5). https://doi.org/10.3390/ma12050686.
- J. Matyas, G.E. Fryxell, B.J. Busche, K. Wallace, L.S. Fifield, Functionalized silica aerogels: advanced materials to capture and immobilize radioactive iodine, 35th International Conference and Exposition on Advanced Ceramics and Composites, Daytona Beach, FL, 2011, pp. 23–32.
- Liu, S.S., Wang, N., Zhang, Y.C., Li, Y.R., Han, Z., Na, P., 2015. Efficient removal of radioactive iodide ions from water by three-dimensional Ag<sub>2</sub>O-Ag/TiO<sub>2</sub> composites under visible light irradiation. J. Haz. Mat. 284, 171–181. https://doi.org/10.1016/ i.ihazmat.2014.10.054.
- Mao, P., Liu, Y., Jiao, Y., Chen, S.W., Yang, Y., 2016. Enhanced uptake of iodide on Ag@ Cu<sub>2</sub>O nanoparticles. Chemosphere 164, 396–403. https://doi.org/10.1016/j. chemosphere.2016.08.116.
- Asmussen, R., Westesen, A., Cordova, E., Yamagata, A., Schonewill, P., Moore, A., Bourchy, A., Saslow, S., Smith, G., Riley, B., Skeen, R., 2023. Iodine removal from carbonate-containing alkaline liquids using strong base resins, hybrid resins, and silver precipitation. Ind. Eng. Chem. Res. https://doi.org/10.1021/acs.iecr.2c03527.
- Kodama, H., 1999. Removal of iodide ion from simulated radioactive liquid waste. Czech J. Phys. 49, 971–977. https://doi.org/10.1007/s10582-999-1026-z.
- Kalinin, N., Elizarova, A., Shchebetkovskii, V., Kuznetsov, Y., Isupov, V., 1983. Leaching of iodine from cement and bitumen compositions containing various iodine compounds. Sov. Radiochem. 25 (4), 505–510.
- Ferry, M., Ngono, Y., 2021. Energy transfer in polymers submitted to ionizing radiation: a review. Rad. Phys. Chem. 180. https://doi.org/10.1016/j. radphyschem.2020.109320.
- Robshaw, T.J., Griffiths, S.M., Canner, A., Bezzina, J.P., Hammond, D.B., Van Meurs, S., Ogden, M.D., 2020. Insights into the interaction of iodide and iodine with Cu(II)loaded bispicolylamine chelating resin and applications for nuclear waste treatment. Chem. Eng. J. 390, 124647–124659.
- Billo, E.J., 2004. Excel for Chemists: A Comprehensive Guide, 3rd ed. John Wiley, Hoboken, New Jersey.
- Revellame, E., Fortela, D., Sharp, W., Hernandez, R., Zappi, M., 2020. Adsorption kinetic modeling using pseudo-first order and pseudo-second order rate laws: a review. Clean. Eng. Technol. 1. https://doi.org/10.1016/j.clet.2020.100032.
- Diniz, C.V., Doyle, F.M., Ciminelli, V.S.T., 2002. Effect of pH on the absorption of selected heavy metal ions from concentrated chloride solutions by the chelating resin Dowex M4195. Sep. Sci. Tech. 37, 3169–3185.
- Wolowicz, A., Hubicki, Z., 2012. The use of the chelating resin of a new generation Lewatit MonoPlus TP-220 with the bis-picolylamine functional groups in the removal of selected metal ions from acidic solutions. Chem. Eng. J. 197, 493–508. https://doi.org/10.1016/j.cej.2012.05.047.
- Ogden, M.D., Moon, E.M., Wilson, A., Pepper, S.E., 2017. Application of chelating weak base resin Dowex M4195 to the recovery of uranium from mixed sulfate/chloride media. Chem. Eng. J. 317, 80–89. https://doi.org/10.1016/j.cej.2017.02.041.
- Onizhuk, M., Panteleimonov, A., Kholin, Y., Ivanov, V., 2018. Dissociation constants of silanol groups of silic acids: quantum chemical estimations. J. Struct. Chem. 59, 261–271. https://doi.org/10.1134/S0022476618020026.

- Pepper, S.E., Whittle, K.R., Harwood, L.M., Cowell, J., Lee, T.S., Ogden, M.D., 2018. Cobalt and nickel uptake by silica-based extractants. Sep. Sci. Tech. 53 (10), 1552–1562. https://doi.org/10.1080/01496395.2017.1405034.
- Lickliss, P.D., 1995. The synthesis and structure of organosilanols. In: Sykes, A.G. (Ed.), Advances in Inorganic Chemistry 42. Academic Press Ltd., London, pp. 147–262.
- Thurlkill, R., Grimsley, G., Scholtz, M., Pace, C., 2006. Hydrogen bonding markedly reduces the pK of buried carboxyl groups in proteins. J. Mol. Biol. 362, 594–604. https://doi.org/10.1016/j.jmb.2006.07.056.
- Asenath-Smith, E., Chen, W., 2008. How to prevent the loss of surface functionality derived from aminosilanes. Langmuir 24, 12405–12409. https://doi.org/10.1021/18802234x.
- Robshaw, T.J., Kearney, S., Turner, J., Simoni, M., Baidak, A., Sharrad, C.A., Walkley, B., Ogden, M.D., 2023. Radioiodine Abatement – Development of radioiodine targeting strategies in the light of Zero Emission Progr. Nucl. Energy 165. https://doi.org/ 10.1016/j.pnucene.2023.104918.
- Duval, Y., Mielczarski, J., Pokrovsky, O., Mielczarski, E., Ehrhardt, J., 2002. Evidence of the existence of three types of species at the quartz-aqueous solution interface at pH 0-10: XPS surface group quantification and surface complexation modeling. J. Phys. Chem. B 106, 2937–2945. https://doi.org/10.1021/jp012818s.
- Adamovich, S., Nalibayeva, A., Abdikalykov, Y., Ushakov, I., Oborina, E., Rozentsveig, I., 2023. New functional alkoxysilanes and silatranes: synthesis, structure, properties, and possible applications. Int. J. Mol. Sci. 24 (18). https://doi.org/10.3390/ iims241813818.
- Wang, L., Chen, Q., Huang, J., Wang, K., Feng, C., Z., 2009. Gen, Synthesis, characterization, and bioactivities of copper complexes with N-substituted Di (picolyl)amines. Trans. Metal Chem. 337–345. https://doi.org/10.1007/s11243-009-9200-5.
- Sole, K.C., Crundwell, F.K., Dlamini, N., Kruger, G., 2018. Mitigating Effects of Silica in Copper Solvent Extraction, 9th Southern African Base Metals Conference. Southern African Institute of Mining and Metallurgy, Livingstone, Zambia.
- Bezzina, J.P., Robshaw, T., Dawson, R., Ogden, M.D., 2020. Single metal isotherm study of the ion exchange removal of Cu(II), Fe(II), Pb (II) and Zn(II) from synthetic acetic acid leachate. Chem. Eng. J. 394, 124862–124872. https://doi.org/10.1016/j. cei.2020.124862.
- Lanford, O.E., Kiehl, S.J., 1941. The solubility of lead iodide in solutions of potassium iodide-complex lead iodide ions. J. Am. Chem. Soc. 63, 667–669.
- Stevenson, J., Sorenson, B., Subramaniam, V., Raiford, J., Khlyabich, P., Loo, Y., Clancy, P., 2017. Mayer bond order as a metric of complexation effectiveness in lead halide perovskite solutions. Chem. Mat. 29, 2435–2444. https://doi.org/10.1021/ acs.chemmater.6b04327.
- Bo, A., Sarina, S., Zheng, Z.F., Yang, D.J., Liu, H.W., Zhu, H.Y., 2013. Removal of radioactive iodine from water using Ag<sub>2</sub>O grafted titanate nanolamina as efficient adsorbent. J. Haz. Mat. 246, 199–205. https://doi.org/10.1016/j. ibazmat.2012.12.008.
- Tauanov, Z., Inglezakis, V.J., 2019. Removal of iodide from water using silver nanoparticles-impregnated synthetic zeolites. Sci. Tot. Env. 682, 259–270. https://doi.org/10.1016/j.scitotenv.2019.05.106.
- Liu, Y., Shen, L., 2008. From langmuir kinetics to first- and second-order rate equations for adsorption. Langmuir 24, 11625–11630.
- Robshaw, T.J., Dawson, R., Bonser, K., Ogden, M.D., 2019. Towards the implementation of an ion-exchange system for recovery of fluoride commodity chemicals. Kinetic and dynamic studies. Chem. Eng. J. 367, 149–159. https://doi.org/10.1016/j. cei.2019.02.135.
- S. Pepper, R.T. J, J.T.M. Amphlett, L.R. Ruder, L.M. Harwood, T.S. Lee, K.R. Whittle, M. D. Ogden, Adsorption of strontium from aqueous solution using ethyl butyl phosphonate (EBP) silica, Progr. Nucl. Energy 177 (2024) 105458. https://doi.org/10.1016/j.pnucene.2024.105458.
- Rarig, R., Hagrman, P., Zubieta, J., 2002. Ligand influences on the structures of copper molybdate chains: hydrothermal synthesis and structural characterizations of [Cu (2,2'-bipyridine)Mo<sub>4</sub>O<sub>13</sub>] and [Cu(2,3-bis(2-pyridyl)pyrazine)Mo<sub>2</sub>O<sub>7</sub>]. Solid State Sci. 4, 77–82.
- Chao, E.E., Cheng, K.L., 1977. The solubility products of some slightly soluble lead salts and the potentiometric titration of molybdate, tungstate, perrhenate and fluoride

- with use of a lead ion-selective electrode. Talanta 24, 247–250. https://doi.org/10.1016/0039-9140(77)80143-4.
- Sing, K., 1982. Reporting physisorption data for gas solid systems with special reference to the determination of surface-area and porosity. Pure Appl. Chem. 54, 2201–2218.
- Ma, H.P., Ren, H., Zou, X.Q., Meng, S., Sun, F.X., Zhu, G.S., 2014. Post-metalation of porous aromatic frameworks for highly efficient carbon capture from  $CO_2 + N_2$  and  $CH_4 + N_2$  mixtures. Polym. Chem. 5 (1), 144–152. https://doi.org/10.1039/c3py00647f.
- McKeown, N., 2017. The synthesis of polymers of intrinsic microporosity (PIMs). Sci. Chin.-Chem. 60, 1023–1032. https://doi.org/10.1007/s11426-017-9058-x.
- Cheng, J., Zou, X., Song, W., Meng, X., Su, Y., Yang, G., Lü, X., Zhang, F., Cao, M., 2010. Effects of concentration of chloride anion on the morphology and microstructure of precipitates from lead nitrate solutions. Cryst. Eng. Comm. 12, 1790–1794. https://doi.org/10.1039/b922594n.
- Song, X., Ma, Y., Wang, C., Dietrich, P., Unger, W., Luo, Y., 2012. Effects of protonation, hydrogen bonding, and photodamaging on X-ray spectroscopy of the amine terminal group in aminothiolate monolayers. J. Phys. Chem. C 116, 12649–12654. https:// doi.org/10.1021/jp302716w.
- Nieto, D., Lindbråthen, A., Hägg, M., 2017. Effect of water interactions on polyvinylamine at different pHs for membrane gas separation. ACS Omega 2, 8388–8400. https://doi.org/10.1021/acsomega.7b01307.
- Olthof, S., Meerholz, K., 2017. Substrate-dependent electronic structure and film formation of MAPbI<sub>3</sub> perovskites. Sci. Rep. 7. https://doi.org/10.1038/srep40267.
- Harland, C.E., 1994. Ion exchange: theory and practice, 2nd ed. Royal Society of Chemistry, Cambridge
- Atkinson, C.M., Walker, G.D., Robshaw, T.J., Rushton, M.J.D., Middleburgh, S.C., Ogden, M.D., 2025. Optioneering in nuclear ion exchange resin disposal. Progr. Nucl. Energy 185, 105719.
- Nair, K.R., Manji, F., Gitonga, J.N., 1984. The occurrence and distribution of fluoride in groundwaters of kenya. East Afr. Med. J. 61 (7), 503–512.
- Yang, H.C., Lee, M.W., Hwang, H.S., Moon, J.K., Chung, D.Y., 2014. Study on thermal decomposition and oxidation kinetics of cation exchange resins using non-isothermal TG analysis. J. Therm. Anal. Calorim. 118 (2), 1073–1083. https://doi.org/10.1007/ s10973-014-3853-9.
- Dubois, M., Dozol, J., Nicotra, C., Serose, J., Massiani, C., 1995. Pyrolysis and incineration of cationic and anionic ion-exchange resins - identification of volatile degradation compounds. J. Anal. Appl. Pyrol. 31, 129–140.
- Gavrichev, K., Bolshakov, A., Kondakov, D., Khoroshilov, A., Denisov, S., 2008. Thermal transformations of lead oxides. J. Therm. Anal. Calorim. 92, 857–863.
- Ren, Y., Liu, S., Duan, B., Xu, Y., Li, Z., Huang, Y., Hu, L., Zhu, J., Dai, S., 2017. Controllable intermediates by molecular self-assembly for optimizing the fabrication of large-grain perovskite films via one-step spin-coating. J. Alloys Comp. 705, 205–210. https://doi.org/10.1016/j.jallcom.2017.01.035.
- Luca, V., Bianchi, H., Allevatto, F., Vaccaro, J., Alvarado, A., 2017. Low temperature pyrolysis of simulated spent anion exchange resins. J. Env. Chem. Eng. 5, 4165–4172. https://doi.org/10.1016/j.jece.2017.07.064.
- Bingham, P., Hyatt, N., Hand, R., 2012. Vitrification of UK intermediate level radioactive wastes arising from site decommissioning: property modelling and selection of candidate host glass compositions. Glass Tech.-Eur. J. Glass Sci. Tech. Part A 53, 83–100
- Bartonicek, B., Habersbergerova, A., Janovsky, I., Kysela, J., Pejsa, R., 1983. Radiolysis of the AV-17X8-CS anion-exchange resin. Rad. Phys. Chem. 22 (3–5), 545–554. https://doi.org/10.1016/0146-5724(83)90062-6.

## **Further reading**

Bezzina, J.P., Robshaw, T.J., Canner, A.J., Dawson, R., Ogden, M.D., 2022. Adsorption studies of a multi-metal system within acetate media, with a view to sustainable phosphate recovery from sewage sludge. J. Environ. Manage. 324. https://doi.org/ 10.1016/j.jenvman.2022.116279.